Urban meteorological forcing data for building energy simulation

Tang, Y., Sun, T. ORCID: https://orcid.org/0000-0002-2486-6146, Luo, Z. ORCID: https://orcid.org/0000-0002-2082-3958, Omidvar, H., Theeuwes, N. ORCID: https://orcid.org/0000-0002-9277-8551, Xie, X., Xiong, J., Yao, R. ORCID: https://orcid.org/0000-0003-4269-7224 and Grimmond, S. ORCID: https://orcid.org/0000-0002-3166-9415 (2021) Urban meteorological forcing data for building energy simulation. Building and Environment, 204. 108088. ISSN 0360-1323 doi: https://doi.org/10.1016/j.buildenv.2021.108088 Available at https://centaur.reading.ac.uk/99057/

Urban meteorological forcing data for building energy simulation

Yihao Tang[*,1,2,3], Ting Sun[*,3,✉], Zhiwen Luo[4], Hamidreza Omidvar[3,4], Natalie Theeuwes[3], Xiaoxiong Xie[4], Jie Xiong[4,5], Runming Yao[4], and Sue Grimmond[3,✉]

[*] These authors contributed equally to this work.

[1] Hunan Key Laboratory for Meteorological Disaster Prevention and Reduction, Changsha, China
[2] Climate Centre of Hunan Province, China Meteorological Administration, Changsha, China
[3] Department of Meteorology, University of Reading, Reading, UK
[4] School of the Built Environment, University of Reading, Reading, UK
[5] Joint International Research Laboratory of Green Buildings and Built Environments (Ministry of Education), Chongqing University, Chongqing, China

[✉] Correspondence: Ting Sun <ting.sun@reading.ac.uk>, Sue Grimmond <c.s.grimmond@reading.ac.uk>

Abstract

Despite building energy use being one of the largest global energy consumers, building energy simulations rarely take the actual local neighbourhood scale climate into account. A new globally applicable approach is proposed to support buildings energy design. ERA5 (**E**uropean Centre **Rea**nalysis version 5) data are used with SUEWS (Surface Urban Energy and Water balance Scheme) to obtain (in this example case) an urban typical meteorological year (uTMY) that is usable in building energy modelling. The predicted annual energy demand (heating and cooling) for a representative four-storey London residential apartment using uTMY is 24.1% less (cf. conventional TMY). New vertical profile coefficients for wind speed and air temperature in EnergyPlus are derived using SUEWS. EneryPlus simulations with these neighbourhood scale coefficients and uTMY data, predict the top two floors have ~40% larger energy demand (cf. the open terrain coefficients with uTMY data). Vertical variations in wind speed have a greater impact on the simulated building energy than equivalent variations in temperature. This globally appliable approach can provide local meteorological data for building energy modelling, improving design for the local context through characterising the surrounding neighbourhood.

Keywords:

EnergyPlus, Urban climate modelling, TMY, Meteorological profiles, Wind profile coefficients, ERA5

1 Introduction

Given the building sector is responsible for about 40% of the global energy use, over 30% of the CO_2 emissions (IEA, 2019), and a third of many countries' total primary energy requirement (PER) (e.g. China 35%, EU 37%, USA 40%; Yang et al., 2014), there is a large effort to reduce energy use in this sector. A

large fraction of this energy is used to maintain thermal comfort. Strategies to reduce energy use (Nazi et al., 2017) and enhance lifetime performance of equipment (Bragança et al., 2014) consider heating, cooling, dehumidification, and ventilation loads (Bourikas, 2016). The design process uses climatological data to assess timing and amount of heating, air conditioning and ventilation systems (HVAC) needed (Herrera et al., 2017; Yao et al., 2011, 2015).

Numerous shortcomings exist to improving building energy modelling for climate resilient design (Hong et al., 2020), here we focus on the climate forcing data. Typically, these data are not *representative* of the neighbourhood that the building will be located in. Atmospheric observations are impacted by their surroundings. If observed outside of the city (e.g., at an airport), the setting is quite different from other neighbourhoods across a city (e.g., low density residential, central business district). Most well-known is the urban heat island effect, where central city near surface air temperatures may stay warmer (cool more slowly) at night than the rural surroundings. With long-term weather stations intentionally located in open vegetated areas, following World Meteorological Organisation (WMO) general siting recommendations, they are unlikely to be representative of urban building sites (cf. Chapter 9 in WMO, 2017) even though the urban expansion may possibly warm the records there (Lowry 1977, Ren et al., 2008; Jones et al. 2008). Urban areas also modify wind (e.g. Grimmond and Oke, 1999), and many other climate variables (e.g. Kershaw et al. 2010, Cleugh and Grimmond 2012, Christen et al. 2004, Offerle et al. 2005, Oke et al. 2017).

Building energy simulation aim to capture the building's response to the outdoor climate. However, the dynamic feedbacks between the buildings and its surroundings (other buildings, vegetation and roads) modify the external atmospheric state, and new buildings in turn impact this (Duan et al., 2019). Notably, heat emissions from buildings (anthropogenic and natural) modify radiation, wind flow, temperatures, *etc*. When these conditions are not considered (e.g., the absence of the urban thermal effects) ventilation systems may neither work as designed, requiring costly retrofit, nor save energy (Short et al., 2004).

Currently, building energy simulations typically use regional climate observations to form a synthetic year from 12 "real" months. Each month is independent, but representative of its long-term mean (e.g. 30 year climatological Normal) (Herrera et al., 2017). Methods to select the months include the so-called *test reference year* (TRY) (Miguel and Bilbao, 2005), and *typical meteorological year* (TMY) (Hall et al., 1978). Although many statistical techniques are used to derive these, they all use observed data from weather stations close to cities, but often in rural/non-urban settings, for varying reference periods (e.g., ASHRAE's (2001) International Weather for Energy Calculations (IWEC), 1982–1999; Zhang and Huang's (2004) Chinese Typical Year Weather, 1982–1997, CMA's (2005) Chinese Standard Weather Data, 1971–2003, CIBSE's UK Test Reference Year, 1984–2013 (Eames et al., 2016)).

To provide the required weather forcing data for building energy simulations at the appropriate scale, many approaches have been taken. These address different issues related to the source of data and spatial scale (e.g., dynamic modelling/downscaling, Murphy (2000)), and the lack of data (e.g. stochastic weather generator, Fatichi et al. (2011); morphing, Belcher et al. (2005)). Among the dynamic modelling approaches two broad categories are CFD (computational fluid dynamics) and urban land surface modelling or urban canopy modelling (UCM, Grimmond et al. 2009). The goal of CFD approaches (e.g., OpenFOAM - e.g. Alibadi et al. (2017); PALM - e.g. Resler et al. (2017), ENVI-Met - e.g. Crank et al. (2018)) is to provide very detailed information at high spatial resolution (O(1 m)), most notably the wind fields. CFD models require high resolution digital surface models and very good model boundary condition meteorology (e.g. downscaled from (or coupled to) numerical weather prediction models). Compared to the UCM approach, CFD is more computationally demanding, and not suitable for climate scale studies spanning decades. The UCM approach utilizes the same type of models as used in numerical weather prediction to parameterise sub-grid scale urban-atmosphere interactions. As these need to be computationally efficient but able to characterise different neighbourhood scale areas (O(0.1 – 10 km)), we take this approach in this study.

The UCM approach tries to capture various aspects of the urban climate caused by modifications of both the landscape form (notably buildings and streets) and people's activities (notably behaviour influencing energy use) (Grimmond et al. 2009, Barlow et al. 2017, Oke et al. 2017, Capel-Timms et al. 2020). A large number range of UCM exist (e.g., Town Energy Balance (TEB) - Masson (2000), single-layer urban canopy model - Kusaka et al. (2001), multi-layer urban canopy model - Kondo et al. (2005), Building Effect Parameterization (BEP) - Martilli et al. (2002), Urban Canopy Parameterisation + Building Energy Model - Salamanca et al. (2009)) to parameterise these net impacts between the urban surface and the atmosphere (as compared in Grimmond et al. 2010, 2011). These models can be run independently (i.e. 'offline') forced by observations, global reanalysis data and/or future climate projections. Reanalysis and climate projections provide spatially continuous data for past and future time periods, respectively. For the latter, a range of scenarios can be modelled. However, the modelled data products (e.g. global reanalysis, future climate) may be at coarse spatial scales and/or not have an urban surface parameterisation within them. Thus, using an offline UCM allows the downscaling of the climate to "any" location accounting for feedbacks from neighbourhood buildings/vegetation/roads and local climate. Underpinning these models is the urban energy balance, which includes anthropogenic heat flux emissions. Near-surface meteorology is diagnosed to provide building energy models with data that incorporate local influences.

Here, our objective is to incorporate the *missing neighbourhood signature* into building simulation data. To demonstrate this, using TMY as the baseline format (but could also be other building energy simulations formats; e.g., Hong et al., 2013; Ohunakin et al. 2013; Sánchez et al. 2020), we use the Surface [Urban] Energy and Water Balance Scheme (SUEWS) (Section 2) to determine neighbourhood scale meteorological variables from a global climate dataset and generate TMY data (Section 3). The neighbourhood-scale TMY data are employed to drive EnergyPlus simulations, whose results are examined against those produced with conventional TMY data (Section 4).

2 SUEWS Enhancement and Evaluation

Surface [Urban] Energy and Water Balance Scheme (SUEWS) is a local-scale land surface model for simulating the surface energy and hydrological fluxes (Grimmond and Oke 1986, 1991; Järvi et al. 2011, 2014; Offerle et al. 2003; Ward et al. 2016) without requiring specialised computing facilities. It has been extensively evaluated and applied in many cities (Lindberg et al. (2018) Table 3, Sun and Grimmond's (2019) Table 1).

2.1 Roughness sublayer atmospheric profiles

In this work we enhance SUEWS (v2020a) to include near-surface diagnostics of meteorological variables in the roughness sublayer (RSL, Fig. 1). The RSL extends from the ground where buildings (and other roughness elements) are located to where their individual influences become blended in the constant flux layer (CFL) or inertial sublayer (ISL, Fig. 1). Knowledge of the atmospheric state within the RSL is required in a wide range of urban service applications (Baklanov et al. 2018, Grimmond et al. 2020) including building energy simulation (e.g. ESP-r (Strachan et al., 2008), TRNSYS (Beckman et al., 1994), and DOE-2 (Lokmanhekim et al., 1979)).

To determine the spatial mean of scalars (e.g., air temperature T, specific humidity q, and wind speed U) or fluxes (e.g., sensible Q_H or latent Q_E heat) we use a RSL approach (Harman and Finnigan, 2007, 2008), assuming: (1) a constant flux layer or ISL above the RSL (Fig. 1), (2) horizontally homogeneous area or neighbourhood, and (3) negligible canopy volume. Standard Monin-Obukhov Similarity Theory (MOST; Monin and Obukhov 1954), assumes that height above the surface is the only relevant length scale within the ISL. When the roughness elements are short and extensive (e.g. vegetation, Fig.1), the RSL is shallow and the ISL extensive because of large fetch. However, in urban areas we are often interested in the processes in the UCL and RSL (Fig.1) so we need to take a RSL approach. For this an additional drag length scale (Coceal and Belcher's 2004 eqn 8) is also used, which is a function of the height of the roughness elements (e.g., buildings, trees) and their spacing. In the urban area, the neighbourhoods (or

fetch) may not be extensive, so the changing UCL and RSL characteristics may make the ISL shallow or even non-existent (Rotach 1999, Cheng and Castro, 2002; Flagg and Taylor, 2011; Britter and Hanna, 2003).

This RSL approach we incorporate into SUEWS was evaluated in Basel and Gothenburg using observations for near neutral to strongly unstable conditions (Theeuwes et al. 2019). Wind speed profiles are better predicted at both sites (cf. a MOST-based approach), and for temperature profiles the results are similar (Theeuwes et al. 2019). The RSL approach provides meteorological values for the UCL and RSL (Fig. 1) that can be used to force building energy simulations.

MOST flux-gradient relations are adapted to the RSL (Garratt, 1980; Theeuwes et al.'s (2019a) Appendix A shows the basis) are used to obtain profiles at height (z), relative to the forcing height (z_a), of T, q and U. For above urban canopy ($z>z_h$):

$$T(z) - T(z_a) \approx \frac{Q_H}{\kappa u_* \rho c_p}\left[\ln\left(\frac{z-z_d}{z_a-z_d}\right) - \psi_H\left(\frac{z-z_d}{L}\right) + \psi_H\left(\frac{z_a-z_d}{L}\right) + \hat{\psi}_H(z) - \hat{\psi}_H(z_a)\right] \quad (1)$$

$$q(z) - q(z_a) = \frac{Q_E}{\kappa u_* \rho L_v}\left[\ln\left(\frac{z-z_d}{z_a-z_d}\right) - \psi_H\left(\frac{z-z_d}{L}\right) + \psi_H\left(\frac{z_a-z_d}{L}\right) + \hat{\psi}_H(z) - \hat{\psi}_H(z_a)\right] \quad (2)$$

$$U(z) = \frac{u_*}{\kappa}\left[\ln\left(\frac{z-z_d}{z_0}\right) - \psi_M\left(\frac{z-z_d}{L}\right) + \psi_M\left(\frac{z_0}{L}\right) + \hat{\psi}_M(z)\right] \quad (3)$$

Within urban canopy layer ($z \leq z_h$):

$$T(z) = T(z_h) - \frac{Q_H}{u_* \rho c_p}\frac{P_r}{\beta f}\left[1 - \exp\left(\frac{\beta f (z-z_h)}{l_M}\right)\right] \quad (4)$$

$$q(z) = q(z_h) - \frac{Q_E}{u_* \rho L_v}\frac{P_r}{\beta f}\left[1 - \exp\left(\frac{\beta f (z-z_h)}{l_M}\right)\right] \quad (5)$$

$$U(z) = U(z_h)\exp\left(\frac{\beta (z-z_h)}{l_M}\right) \quad (6)$$

where κ is the von Kármán constant (0.4), u_* friction velocity, ρ density of air, c_p the specific heat of air at constant pressure, L_v the latent heat of vaporisation, P_r the Prandtl number, and l_M the mixing length. β and f are the Harman and Finnigan (2007) parameters. For the surface roughness length for momentum (z_0), zero-plane displacement (z_d), the integral form of stability correction function for momentum, heat, water vapour (ψ_m, ψ_h, ψ_v), and the correction functions for the RSL effects from the urban roughness elements ($\hat{\psi}_m$, $\hat{\psi}_h$ and $\hat{\psi}_v$) forms are based on Harman and Finnigan (2007) as given in Theeuwes et al. (2019a). Potential temperature ($\theta = T\left({}^{p_0}/_{p}\right)^{R/c_p}$; actual ($p$) and standard atmospheric pressure (p_0 =100 kPa), gas constant for air (R)) is needed in eqn 4 if there are large height differences (e.g. > 200 m, ~2.1 kPa equivalent in air pressure), but otherwise it is acceptable to use air temperature T instead of θ

(Brutsaert 1982).

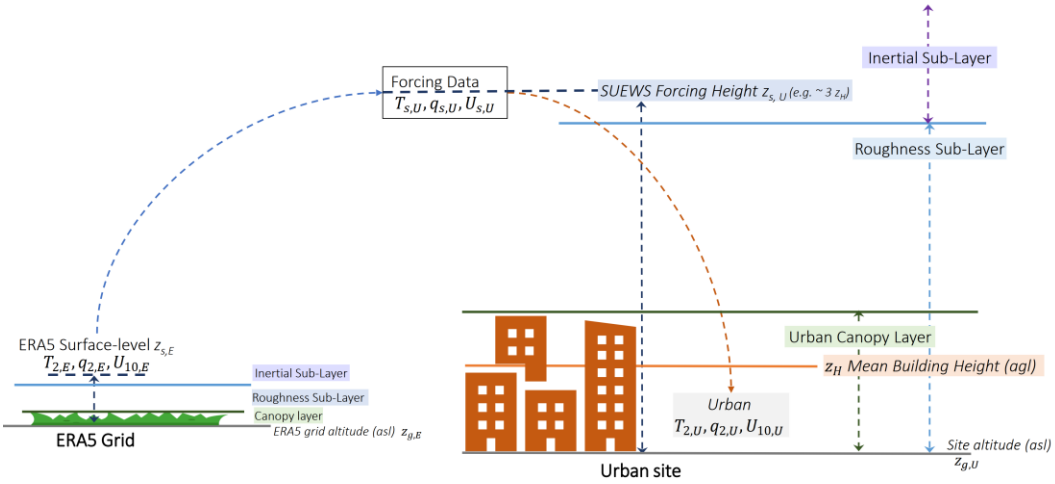

***Figure 1**: Over a simple extensive vegetated surface, the roughness elements (plants) create the canopy layer. In an urban neighbourhood the roughness elements (e.g. buildings and trees) create the urban canopy layer (UCL). In both areas critical layers of the atmosphere and their approximate heights are indicated. The ERA5 surface-level data (Section 3.1) are assumed to represent environment with short vegetation (roughness length for momentum $z_{0m,E}$ = 0.3 m, Hersbash et al. 2020). As the vegetation is short the effect of the individual plants is blended so 'sensor' height is within the inertial sublayer (ISL) or constant flux layer (CFL). The spacing and height of urban roughness elements influences the depth of the urban RSL. The SUEWS forcing height ($z_{s,U}$) needs to be within the ISL. Variations in meteorological variables (notably temperature, pressure, humidity) are impacted by altitude differences (above sea level, asl) between areas. The SUEWS RSL module (Eqn. 1–6) determine the variables (air temperature T, specific humidity q and wind speed U) within the RSL for a height of interest for an application. Figure not to scale.*

2.2 Evaluation of the temperature profiles: methods and results

SUEWS ability to predict energy and water fluxes in central London has been evaluated (e.g. v2016: Ward et al. 2016; v2017a, Ward and Grimmond 2017) using eddy covariance and radiation sensors mounted in the ISL (Fig. 1) to measure these fluxes (Kotthaus and Grimmond 2014). This is complemented by profile data into the UCL (Björkegren and Grimmond 2018). These data are used to evaluate SUEWS v2020a with a focus on the performance in predicting vertical temperature profile given it is a key enhancement in this new version with the RSL module.

Buildings are the predominate land cover (Fig. 2; Table 1) in this area. The SUEWS model configuration draws upon Ward et al. (2016), using the physics schemes indicated in Table 2. Gap-filled meteorological observations for 2013, from sensors located at 49.6 m on a lattice flux tower are used as forcing. The evaluation uses two fine wire thermocouples sensors (6.5 and 12.5 m agl, 30 min averages) with data available for two periods (1 January – 18 March 2013 and 28 April to 27 June 2013). These sensors are located below roof level (mean building height 21.5 m, Kotthaus and Grimmond 2014) in the UCL. The SUEWS simulations are conducted with a 5 min timestep for two years (2012–2013) with the first year as

spin-up.

The simulation results are aggregated into 30 min averages for evaluation. The metrics used for this are the mean absolute error (MAE) and mean bias error (MBE). Both have units of the variable and would be ideally 0 ºC. The interquartile range (IQR) with the median allows the variability between 25th and 75th percentile relative to 50th percentile to be compared.

The data are evaluated for a series of different conditions during the period:
(1) *Sunny*: [measured incoming solar radiation to top at the atmosphere] ratio > 0.65.
(2) *Cloudy*: non-sunny days without rain.
(3) *Rainy*: daily total precipitation > 3 mm d^{-1}
(4) *Windy*: daily mean wind speed > 2 m s^{-1}
(5) *Weekday*: Monday to Friday
(6) *Weekend*: Saturday to Sunday

At both positions in the UCL the simulated 30 min mean air temperature for the evaluation periods have MAE of less 1 ºC (Fig. 3). The median diurnal cycles (and inter quartile range) are consistent with the observed values (Fig. 3a, d). The MBE indicates the simulated air temperatures are slightly underestimated at both heights (Fig. 3b, e).

The results for 6.5 m agl are better simulated on sunny than cloudy days (Fig. 3c). At both heights, the model performs better during weekdays than for weekends (Fig. 3c, f). When other conditions are assessed the model performance is similar (Fig. 3c, f). Overall, SUEWS-RSL has reasonable skill in predicting sub-daily dynamics of near surface air temperature.

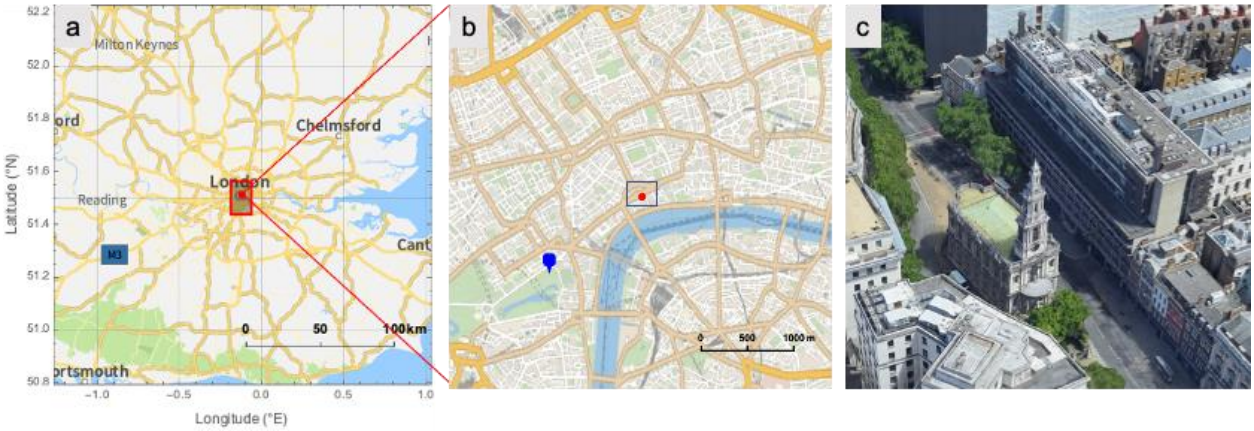

***Figure 2**: SUEWS evaluation site: (a) within Southeast England with ERA5 (Section 3.1) 0.125° × 0.125° (~12.5 km) grid (red box), (b) simulation site (red dot) and St James's Park (blue marker) within central London, and (**c**) oblique view of the canyon. Sources: (a-b) OpenStreetMap (2017); (c) Google (2021).*

***Table 1**: Plan area fractions surrounding the central London site within the average footprint climatology derived by Kotthaus and Grimmond (2014).*

Site	Plan area (fraction)						
	Building	Paved	Evergreen Trees	Deciduous Trees	Grass	Bare Soil	Water
KC	0.43	0.38	0.00	0.02	0.03	0.04	0.14

***Table 2**: SUEWS used with options selected as defined in Sun et al. (2020). Sun et al. (2021) gives the model setup and all model results*

Physics scheme	Code	Remark
Radiation	3	Net all-wave radiation: incoming longwave radiation modelled uses air temperature and relative humidity (Loridan et al., 2011)
Heat storage	1	OHM model (Grimmond et al., 1991)
Anthropogenic heat	2	Anthropogenic heat model responds to temperature and population density based on time of day and day of week (Järvi et al., 2011) with heating set point $T_H = 18\ °C$ and cooling $T_C = 26\ °C$.
Snow	0	Snowpack modelling with radiative, thermal, hydrological, and human dynamics (Järvi et al., 2014)
Roughness length for momentum	2	Momentum roughness length and zero plane displacement height: function of height (Grimmond and Oke, 1999)
Roughness length for heat	2	Thermal roughness length: function of vegetation fraction with bluff bodies (Kawai et al., 2009)
Atmospheric stability	3	Atmospheric stability correction function (Campbell and Norman, 1998)

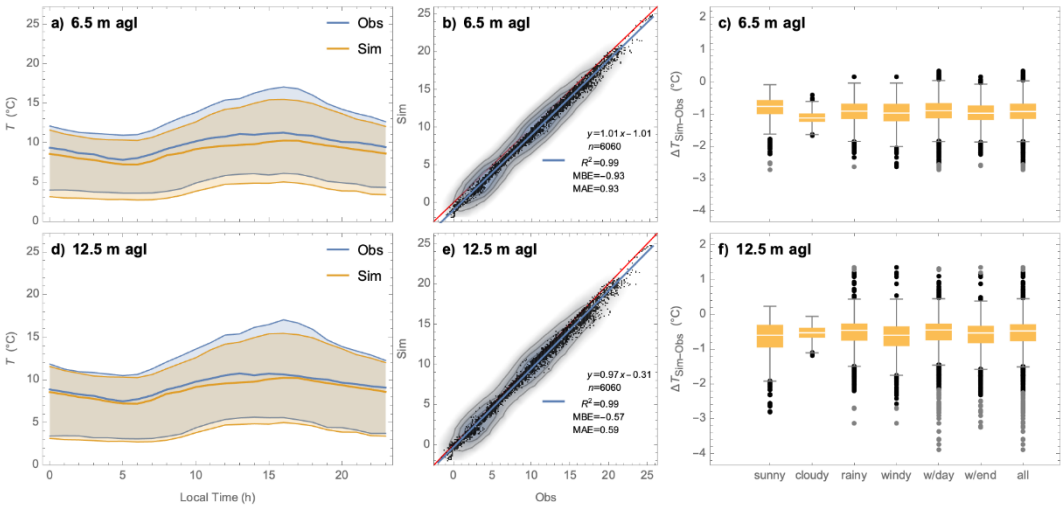

***Figure 3**: Air temperature simulated with SUEWS-RSL and observed at two heights (6.5 and 12.5 m agl) in central London (Fig. 2) during the periods 1 January – 18 March 2013 and 28 April to 27 June 2013: **(a, d)** diurnal median (line) and inter-quartile range (IQR, shading); **(b, e)** 30 min data (black) with data density (shading > 1/1000 of probability density function); and **(c, f)** box plot 30 min bias between simulations and observations (IQR, median with 5th and 95thpercentiles whiskers, outliers (dots) for classification criteria given in Section 2.2).*

3 Building energy simulations methods

To assess the impacts of using different climate data (uTMY, cTMY and uAMY) on building energy load simulations we use the heating-cooling (HC) mode in EnergyPlus. As our study goal is *not* design optimization, we select one common building archetype that occurs in Greater London (Communities and Local Government 2008, Three Regions Climate Change Group 2008, Porritt 2012) rather than anything representative of actual buildings around the site used in the SUEWS evaluation (Section 2).

3.1 Configuration for Climate Runs

In this study, we use the ERA5 (**E**uropean Centre **Rea**nalysis version 5) data as our source of meteorological variables, as it is globally available at 0.125° × 0.125° (~12.5 km) resolution, and at hourly resolution from 1979 to within 5 days of real time (Hersbach et al., 2020). We use the ground level (Fig. 1) data ($z_{s,E}$), which in ERA5 is typically assumed to be similar to the standard WMO observational area of extensive short grass, so the RSL/ISL boundary is close to the ground (a typical 2 m agl observation within the ISL, Fig. 1).

To force SUEWS the meteorological data need to be at an equivalent height above the roughness elements ($z_{s,U}$, Fig. 1, i.e. above the RSL). Roughness element heights and spacing influence $z_{s,U}$ (e.g. references within Grimmond and Oke 1999, Kastner-Klein and Rotach 2001, Grimmond et al. 2004, Ao et al. 2018). In this study, we use $3z_H$ as the area has a dense building canopy (Oke et al. 2017).

To adjust the data two height differences (Fig. 1) need to be accounted for:

$$\Delta z_{net} = \Delta z_g + \Delta z_s = \left[z_{g,U} - z_{g,E}\right] + \left[z_{s,U} - z_{s,E}\right] \quad (7)$$

(1) *altitude* Δz_g (height above sea level, asl) between the site of interest ($z_{g,U}$) and ERA5 grid altitude ($z_{g,E}$). In areas with large terrain variability over short distances this can be significant.
(2) *surface roughness elements* Δz_s (height above ground level, agl).

3.2 Generation of urban Typical Meteorological Year (uTMY)

To force building energy simulations, one common data type is TMY. The general method used to select these data is outlined in Appendix A. We refer to this as the conventional TMY (cTMY) (Fig. 4).

Here we also generate a dataset with local-scale neighbourhood effects accounted for, that we refer to as our urban TMY (uTMY) dataset. To generate this the following steps are used (Fig. 4), that correspond to Appendix A steps (*c#*) as indicated:
(*u1*) *Meteorological variables selection* (step *c1*)*:* air temperature T_a, relative humidity RH, wind speed U and incoming shortwave radiation $K_{\downarrow}$.

(*u2*) *Data source selection* (step *c2*)*:* ERA5 (Hersbach et al., 2020) data (Section 3.1) are used, which is refer hereafter to as Actual Meteorological Years (AMY).

(*u3*) *Urban climate modelling:* SUEWS (Section 2) is used to obtain the neighbourhood scale forcing variables (e.g., air temperature, humidity, wind speed). These create an urban AMY dataset (uAMY, a multi-year climate series with same timespan as source data chosen in *u2*).

(*u4*) Selection *of months* (steps *c3* and *c4*): We use the Hall et al.'s (1978) weights (w_v) in eqn A2 for both cTMY and uTMY. However, despite $w_{K_\downarrow} = 0.5$ (Table A.1) we keep uAMY $K_\downarrow$ and AMY $K_\downarrow$ the same, as spatially variability from clouds over short distances creates observations and modelling challenges (e.g., Dastoor, 1994; Forbes and Ahlgrimm, 2014).

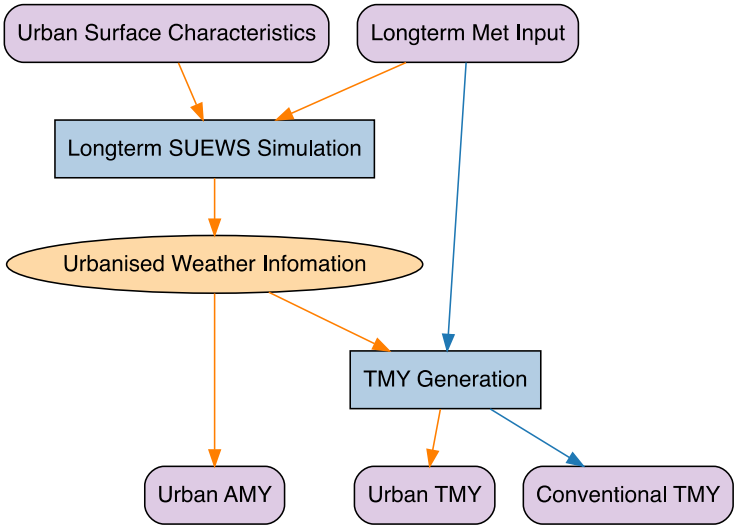

Figure 4*: Workflow to generate urban (u) typical meteorological year (uTMY, orange arrows) and conventional TMY (cTMY, blue arrows) datasets from actual meteorological year (AMY) data.*

3.3 EnergyPlus Configuration

The open-source building energy simulation programme funded by the U.S. Department of Energy, EnergyPlus, integrates multiple modules of building systems to simulate thermal zones based on heat balance models (Crawley et al., 2001). For the energy balance of building zone air, the model considers: convective internal loads; convective heat transfer from the zone surfaces; heat transfer from inter-zone air mixing; heat transfer from infiltration of outside air; and hot or cold air from mechanical systems to the zones to meet heating or cooling loads.

The heating and cooling energy loads are simulated for the 'low-rise residential flat' archetype (Fig. 5, Table 3) in Greater London. The description is derived from various sources (Communities and Local Government 2008, Three Regions Climate Change Group 2008, Porritt 2012). The building's main façade has a north-south orientation (Fig. 5a). Each floor has two flats and a shared hallway (Fig. 5b). Each flat

is modelled with five thermal zones. The building is sited in an infinite plane without surrounding buildings, which will impact surface fluxes (e.g. Xie et al. 2021).

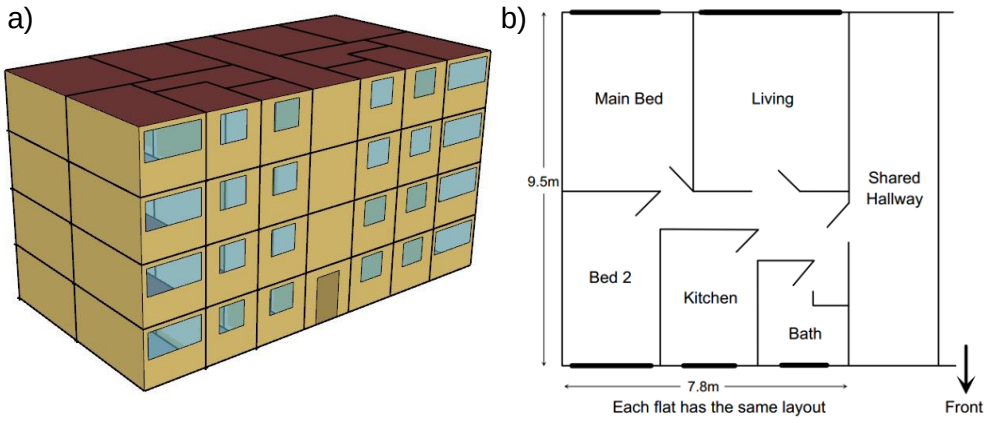

Figure 5*: EnergyPlus simulations are undertaken for (a) a low-rise flat in Greater London with (b) floor plan (height of floor: 2.5 m) based on details from Communities and Local Government (2008) and Three Regions Climate Change Group (2008).*

Table 3*: Parameters used in the EnergyPlus simulations for a low-rise residential flat in Greater London (Porritt, 2012). Configuration files can be found in Sun et al. (2021).*

Parameters	**Specifications**
U-value (W m^{-2} K^{-1})	External wall = 1.37 External window = 2.70 (Pre-2002 double-glazing)
Window to wall ratio	North = 0.29, South = 0.23, East = West = 0
Ventilation and infiltration	Dynamic, calculated with opening area and pressure difference (cf. Fig. S1)
Occupant density (m^{-2})	0.04
Activities and occupied hours	Sitting (living room: 7:00 to 9:00 and 17:00 to 23:00): 108 W $person^{-1}$ Sleeping (bedroom: 23:00 to 7:00): 72 W $person^{-1}$
Energy consumption (W m^{-2})	Lighting = 4.1, Equipment=4.0
Heating/cooling point (°C)	18 / 26
Cooling/Heating mode	Continuously operating when indoor temperature is beyond the thermal comfort range using ideal HVAC system

Three model runs are undertaken with different meteorological forcing data of varying timespan (Table 4): the cTMY is generated following steps in Appendix A while uTMY is produced after procedure in Section 3.2; uAMY is the urbanised actual meteorological years from 1979 to 2020, representing the past truth.

The cTMY data are estimated for the WMO standard observing reference heights (i.e., 2 m agl for T and RH, 10 m for U) (Table 4). These standard WMO heights, although used in many applications, are much shorter than the mean building height in almost all urban areas. Here our focus is on an area of central London (Fig. 2) with a mean building of 21.3 m (Kotthaus and Grimmond 2014). Hence, both (wind, temperature) WMO reference heights are well within the urban canopy layer (Fig. 1).

Analysis of the EnergyPlus results (Section 4) uses the net values for the four floors, unless otherwise indicated. The impact of buildings on the variables profile, and on building energy simulations are discussed in Section 4.3.

Table 4: *Summary of EnergyPlus simulations undertaken. The forcing heights are based on WMO standard observations heights (i.e., 2 m agl for temperature and relative humidity, 10 m for wind) (Fig. 1). The uTMY data are also used for the Table 6 model runs.*

Meteorological data	Forcing height	Period
cTMY	WMO	12 months selected from 1979–2020
uTMY	WMO	12 months selected from 1979–2020
uAMY	WMO	All months of 1979–2020

4 Results and Discussion

4.1 Comparison of the conditions within the uTMY and cTMY

First, we examine the characteristics of the months selected in the two TMY datasets (Table 5) derived for one 0.125°×0.125° grid in central London (51.0°N, 0.125°W, Fig. 2) from ERA5 data for 1979-2020 (Hersbach et al. 2020). As the climate variables differ between uTMY and cTMY (i.e., with and without urban characteristics), different months may be selected (Appendix A).

However, if the final decision is between the same five candidates, the non-changed incoming solar radiation (Section 3.2, Appendix A) will result in the same period being chosen. Here, only April differs (Table 5, orange shading) from the four months with different candidate years (Table 5, blue shading), despite June having more different candidate years. However, April is the only month for which the 1st candidate differs.

The actual time series of variables differ between the two TMY even when the same months are selected (Fig. 6). Overall, the temperatures are comparable (Fig. 6a–d) with an hourly mean absolute difference of <0.6 °C in each season. The ERA5 dataset utilises actual observations with the ECMWF Integrated Forecasting System (IFS) meteorological model via data assimilation (Hersbash et al. 2020). Thus, despite the IFS not having an urban land surface model any data assimilated that are measured within a city will have an urban signature (e.g. air temperature measured at St James's Park in central London, blue marker in Fig. 2b). The ERA5 data are assumed to represent short vegetation ($z_{0m,E}$ = 0.3 m, Hersbash et al. 2020) at the latitude and longitude of the grid cell but this would be inappropriate for an urban setting. The uTMY T has a mean bias error of −0.53 ℃ (cf. cTMY, Fig. 6a, b), indicating a counter-intuitive cooler T than cTMY.

As uTMY accounts for the neighbourhood mean building heights the ERA5 data are lapse-rate corrected (Appendix B, Fig. 1) for height differences (eqn 7). However, the environmental lapse rate (−6.5 K km^{-1}) used may possibly be too large for central London (Dutra et al. 2020). These corrected data are used to

force SUEWS-RSL, to obtain near surface (in this case 2 m) air temperature within the UCL accounting for the surroundings (Table 1). The cTMY, because of the ERA5 data assimilation, have an inherent urban signature. Obviously these both differ from using the IWEC data for Gatwick Airport (ASHRAE 2001). These differences imply the heterogeneity in a megacity like London, warrants attention in TMY generation.

The wintertime *RH* values are larger (> 80%) than the other seasons (Fig. 6c). Wind speeds are reduced in the uTMY (cf. cTMY, Table 5) across all seasons (Fig. 6e), with an MBE of about -2 m s^{-1}. Differences in $K_{\downarrow}$ between cTMY and uTMY (Fig. 6g) occurs only in one month (Table 5) as no other corrections are done (Appendix B). Although, such corrections are important in building energy simulations (e.g. Xie et al. 2021).

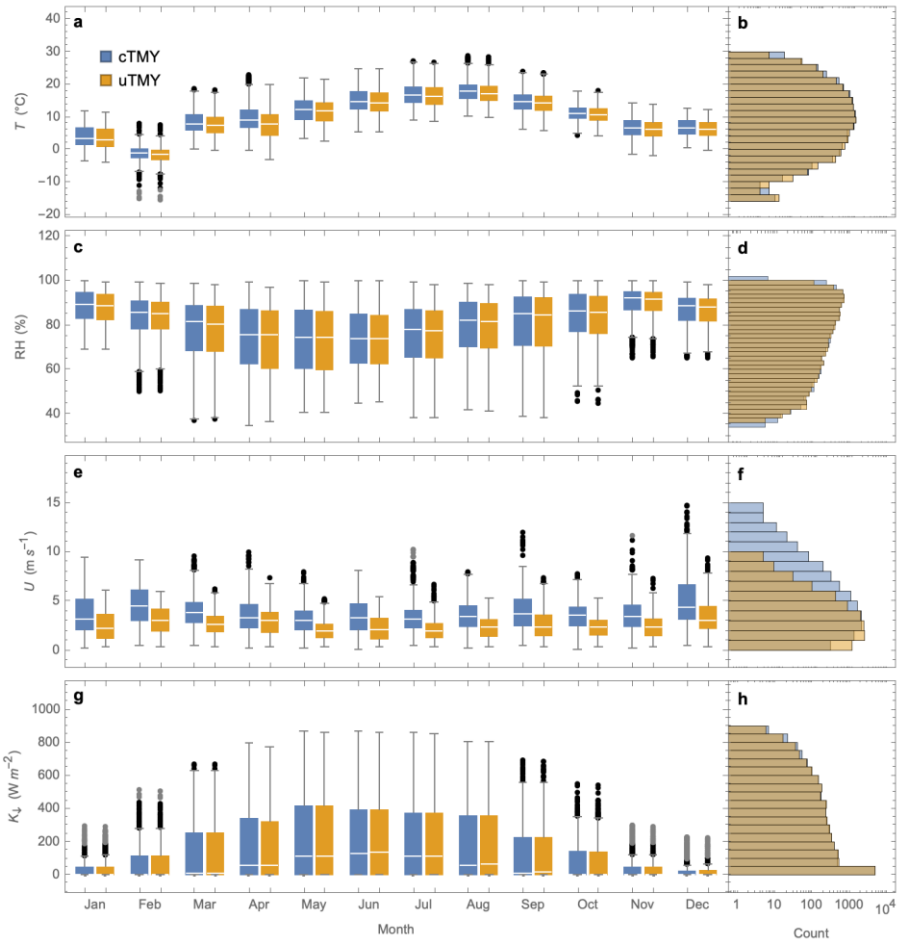

***Figure 6**: Monthly boxplots (as Fig. 3c,f) and frequency (logarithmic scale) for uTMY (gold) and cTMY (blue) for: (**a–b**) air temperature T, (**c–d**) relative humidity RH, (**e–f**) wind speed U and (**g–h**) incoming solar radiation $K_{\downarrow}$.*

***Table 5**: Top five years selected from 1979-2020 ERA5 data with metrics W (dimensionless, eqn A.2) and RMSD ($W\ m^{-2}$) (eqn A.3) values for each month (M), used to construct cTMY and uTMY datasets. Selection of different candidate years between the cTMY and uTMY (blue shading) and final chosen month (orange shading) indicate few differences.*

	cTMY Year ***W*** **| RMSD**					**uTMY Year** ***W*** **| RMSD**				
M	1st	2nd	3rd	4th	5th	1st	2nd	3rd	4th	5th
1	1992 0.267 | 11.1	2013 0.271 | 13.6	2015 0.235 | 13.6	2006 0.252 | 14.2	2001 0.269 | 16.8	1992 0.263 | 11.1	2013 0.270 | 13.6	2015 0.235 | 13.6	2006 0.252 | 14.2	1982 0.271 | 14.4
2	1986 0.250 | 22.5	1997 0.253 | 25.1	2002 0.243 | 27.4	2001 0.247 | 27.5	2019 0.243 | 31.3	1986 0.250 | 22.5	1979 0.251 | 24.4	2002 0.243 | 27.4	2001 0.250 | 27.5	2019 0.240 | 31.3
3	2014 0.247 | 38.7	1997 0.250 | 40.7	1986 0.252 | 41.3	2012 0.211 | 47.2	2003 0.221 | 50.9	2014 0.248 | 38.7	1997 0.251 | 40.7	1986 0.253 | 41.3	2012 0.212 | 47.2	2003 0.220 | 50.9
4	2019 0.245 | 51.3	1987 0.225 | 52.9	2015 0.247 | 59.5	2011 0.239 | 60.7	1984 0.220 | 64.8	2013 0.247 | 43.9	2019 0.244 | 51.3	1987 0.223 | 52.9	2011 0.240 | 60.7	1984 0.225 | 64.8
5	2019 0.269 | 52.7	2003 0.273 | 55.6	1993 0.270 | 59.3	2001 0.264 | 69.2	1996 0.275 | 75.1	2019 0.267 | 52.7	2003 0.271 | 55.6	1993 0.267 | 59.3	2014 0.274 | 68.6	2001 0.264 | 69.2
6	1984 0.258 | 42.7	1999 0.270 | 62.5	2012 0.228 | 65.7	1986 0.262 | 75.5	1994 0.270 | 77.1	1984 0.258 | 42.7	1990 0.270 | 55.6	2005 0.269 | 64.9	2012 0.227 | 65.7	1986 0.265 | 75.5
7	2004 0.257 | 50.5	2010 0.236 | 52.1	1994 0.265 | 61.1	2019 0.268 | 65.0	1993 0.259 | 65.7	2004 0.254 | 50.5	2010 0.235 | 52.1	1994 0.268 | 61.1	2019 0.268 | 65.0	1993 0.258 | 65.7
8	2004 0.242 | 48.0	2015 0.234 | 54.7	2018 0.240 | 58.9	1995 0.248 | 67.3	2003 0.235 | 67.8	2004 0.239 | 48.0	2015 0.234 | 54.7	2018 0.245 | 58.9	1995 0.248 | 67.3	2003 0.235 | 67.8
9	1981 0.234 | 35.9	1997 0.225 | 40.7	1999 0.235 | 45.9	2004 0.204 | 46.7	1991 0.205 | 50.9	1981 0.235 | 35.9	1997 0.228 | 40.7	1999 0.235 | 45.9	2004 0.205 | 46.7	1991 0.208 | 50.9
10	2016 0.230 | 20.8	1991 0.221 | 26.0	1979 0.231 | 28.6	1986 0.238 | 32.7	1994 0.246 | 33.2	2016 0.232 | 20.8	1991 0.226 | 26.0	1985 0.248 | 26.6	1979 0.231 | 28.6	1986 0.238 | 32.7
11	2019 0.254 | 14.0	2014 0.244 | 14.3	1991 0.252 | 15.7	1985 0.216 | 16.4	2018 0.241 | 17.1	2019 0.251 | 14.0	2014 0.245 | 14.3	1991 0.251 | 15.7	1985 0.215 | 16.4	2018 0.239 | 17.1
12	2013 0.264 | 10.9	1984 0.270 | 12.6	1983 0.258 | 12.7	1999 0.254 | 13.1	1995 0.271 | 13.8	2013 0.262 | 10.9	1984 0.273 | 12.6	1983 0.261 | 12.7	1999 0.254 | 13.1	1995 0.270 | 13.8

4.2 Impact of climate forcing on the building energy simulations

Using the uTMY and cTMY data, the energy loads for the residential building (Fig. 5) are modelled with EnergyPlus (Section 3.3). Although London rarely has air conditioning installed it is permitted in this simulation. A consistently higher energy load is predicted from cooling (although minimal, <7 kWh m^{-2} in total for both cases) with uTMY (cf. cTMY) but lower heating load, particularly in winter months (November to February) (Fig. 7). The uTMY forcing data predicted higher cooling (44.6 %) demand is offset by the decrease in heating (11.5%) to give a net annual decrease of 6.9% (Supplementary Material Fig. S2a).

More generally, seasonal and net annual differences obviously depend on regional climate because of geography (e.g. latitude, maritime/continental). However, the urban wind speeds are expected to be notably lower and will have uneven but clear impacts on energy load in different seasons. Such intra-annual differences may exert a non-trivial influence on the energy load.

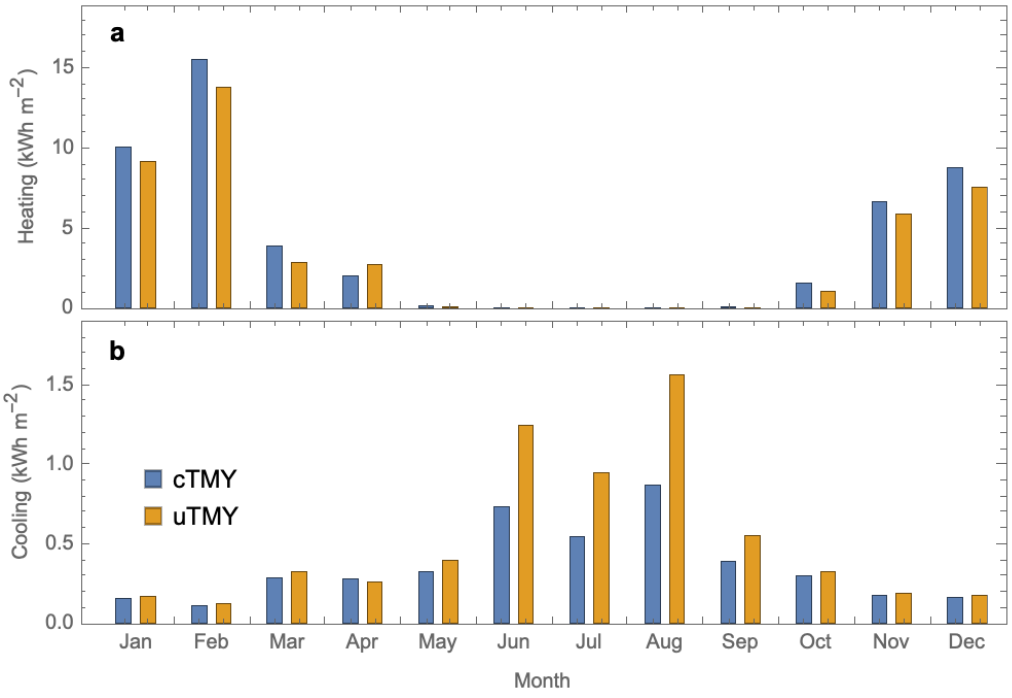

Figure 7*: Monthly EnergyPlus energy load simulated for central London (a) heating and (b) cooling using two TMY datasets (Table 4). Supplementary material Fig. S2 shows daily scale cumulative annual influence.*

If all available climate data are used (i.e., the long-term ERA5 data since 1979, with urban characteristics, uAMY, Table 4) the variability caused by climate can be assessed. The annual total energy load differs between the three datasets by season (Fig. 8a), with the uTMY results more similar to the uAMY than cTMY. The annual uTMY results are closer to the uAMY median (10.1% difference, e.g. [(uTMY − $uAMY_{med}$) × 100]/ $uAMY_{med}$) than cTMY (18.3%) (Fig. S2a). As these results are consistent with

previous TMY modelling studies (e.g. Cui et al., 2017), it suggests more attention is warranted into the method of selecting typical months. However, it is promising that uTMY estimates the building energy load with better agreement to uAMY across all seasons (cf. cTMY).

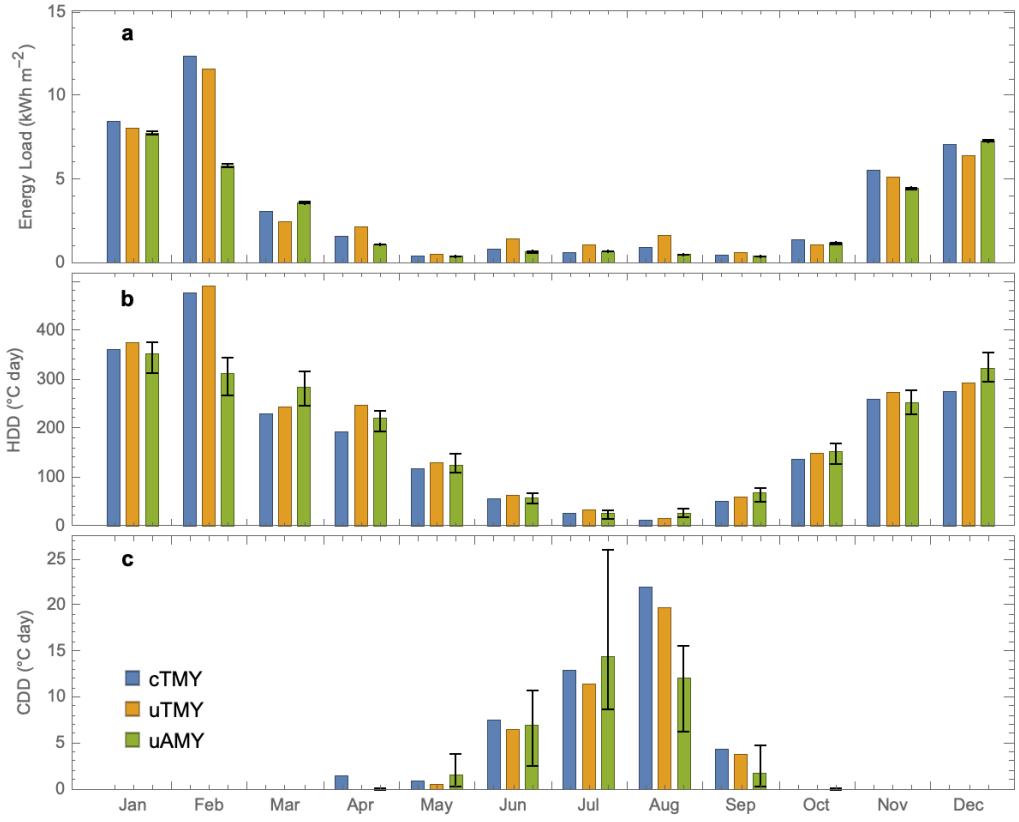

***Figure 8**: Using cTMY, uTMY and uAMY to determine monthly total: (a) heating degree days (HDD) and (b) cooling degree days (CDD). Error bars for uAMY show ranges between the 25th and 75th percentiles. Supplementary material Fig. S2 shows daily scale cumulative annual influence.*

Given the simple and popular use of heating degree days (HDD) and cooling degree days (CDD) as proxies of potential heating (cooling) energy load, we calculate these with base temperature of 15.5 °C (18 °C) (CIBSE 2006). Unlike the EnergyPlus predictions (Fig. 8a), the HDD (Fig. 8b) results suggest the cTMY is better than uTMY at representing the median uAMY (Fig. S2b). Whereas for the CDD, uTMY is better than cTMY overall but the pattern of timing of days is poor in both TMY (Fig. 8c, S2c), likely suggesting quite different type of solution needs. The EnergyPlus building energy simulations, appear to differ most in the early spring (Fig. 8a, S2a), which indicates they are the more useful and consistent estimate of building energy load independent of the three sources. This suggests use of temperature-only-based proxy indicators (e.g. HDD/CDD) are not representative of the median TMY climatology.

4.3 Impacts of vertical meteorological profiles on building energy simulations

Meteorological conditions vary with height, but a TMY dataset only contain values for one height. Given

a single storey building, the standard 2 m level is approximately half building height but for taller buildings an increasing fraction of the building volume is above that. Here we consider the impact on the vertical variation in meteorological conditions on building energy simulation. The wind speed and air temperature are modified from (ASHRAE 2005):

$$U_{s,z} = U_{10}\left(\frac{\delta_{ref}}{z_{10}}\right)^{\alpha_{ref}}\left(\frac{z_s}{\delta}\right)^{\alpha} \quad (8)$$

$$T_{s,z} = T_2 + \Gamma(z_s - z_2) \quad (9)$$

where δ is referred to as the boundary layer depth (Table 6). In the EnergyPlus, this refers to the height where a constant mean gradient wind speed is assumed to occur (Gupta and Moss, 1993), rather than the meteorological "boundary layer depth" that varies through the day and season (e.g., Kotthaus and Grimmond 2018). By default EnergyPlus uses open terrain values (δ_{ref} = 270 m, α_{ref} = 0.14, ASHRAE (2005), Table 6) with 10 m agl wind speed and 2 m agl air temperature reference levels.

As these profiles (eqn 8, 9) are recommended by ASHRAE (2005), they are widely used in building energy simulations. Comparison of these to the RSL-based predictions (eqn 6, 4) have obvious differences (Fig. 9). The SUEWS-RSL urbanised meteorology (median values at each height with 8760 hourly results under all conditions, shown in central dashed red lines in Fig. 9) are used to derive coefficients (Table 6) for use in EnergyPlus eqn 8 profiles (Fig. 9a. red solid lines) using NonlinearModelFit of Mathematica v12.2 (Wolfram Research 2008). For temperature, a new near surface lapse rate is determined for eqn 9 from the RSL analyses (Table 6, Fig. 9b). The corrected coefficients are considered more appropriate for a central business district similar to central London.

Table 6*: Coefficients for Eqn. 8 and 9. The default EnergyPlus values (*) are for open terrain. SUEWS-RSL results fitted parameters are provided with standard errors at a 95% confidence level.*

Terrain	**Exponent α**	**Boundary layer depth δ (m)**	**Lapse rate Γ (K km^{-1})**	**Source**
Open*	0.14	270	6.5	*ASHRAE 2005*
Rough	0.22	370	6.5	*ASHRAE 2005*
Urban	0.33	460	6.5	*ASHRAE 2005*
Central business district	0.29 ± 0.03	50.1 ± 8.3	1.6 ± 0.03	UT; This study Fig. 9
Central business district	0.29 ± 0.03	50.1 ± 8.3	6.5	U; This study Fig. 9a
Central business district	0.14	270	1.6 ± 0.03	T; This study Fig. 9b

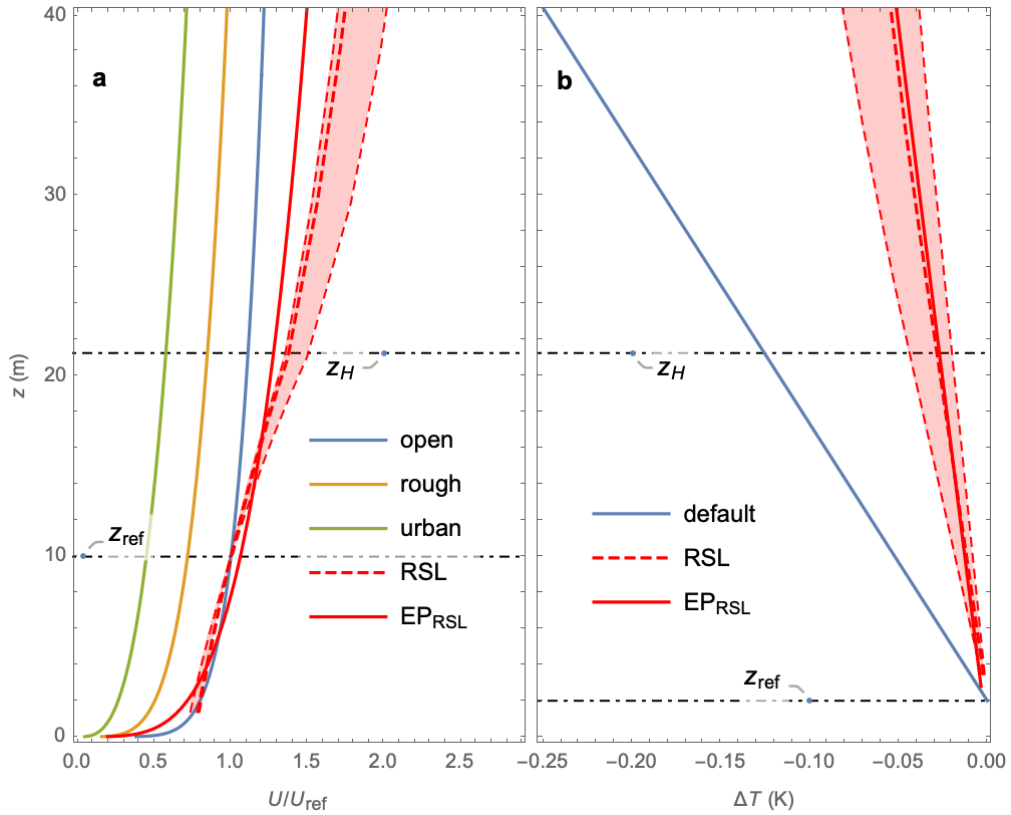

***Figure 9**: Mean building height (z_H) (Fig. 2) and vertical profiles of: (**a**) wind speed (eqn 8, Table 6 coefficients, eqn 3 RSL) normalised by wind speed at 10 m agl (z_{ref}), and (**b**) air temperature (eqn 9, Table 6 coefficients, eqn 1 RSL) difference 2-m agl (z_{ref}) temperature. The annual median (line) and interquartile range (shading) are shown using uTMY data.*

The RSL-based corrections lead to differences in wind speed and air temperature of varying magnitude across all floors with the top floor (f3) having the largest differences (Fig. 10) when eqn 8 and 9 are used with open terrain coefficients (Table 6). Both wind speed and air temperature differences increase with the height above ground.

New coefficients for eqn 8 and 9 are derived using the RSL data (Fig. 9) for three conditions: wind and temperature together (denoted by UT), but also for each separately to understand their roles (i.e. U and T) (Table 6). These are used in EnergyPlus with the uTMY data to examine the impacts on energy load for different floors in the residential building.

The energy loads for the top two floors (f2 and f3) show the largest changes when different coefficients are used (Fig. 11). Accounting for wind speed has a generally larger impact (> ~8% in all cases; Fig. 11), with larger influences at higher floors (> 9%). Wind speed corrections dominate the impact (UT, U, cf. T Fig. 11) whereas, the temperature-correction-induced changes are very minimal (< 1% in all cases), suggesting the relative minor role of temperature in the case examined here.

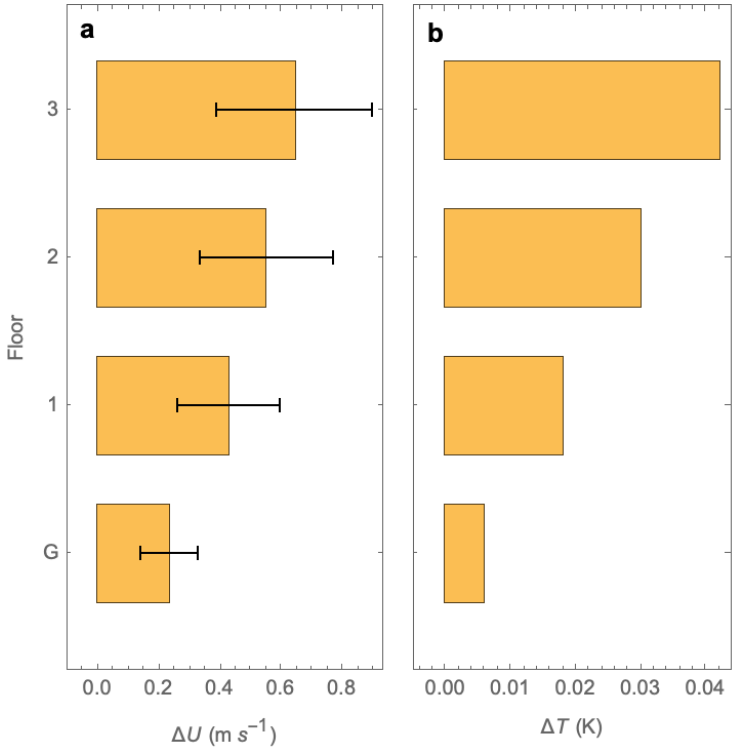

***Figure 10**: Median difference in calculated: (a) wind speed (eqn 8 – eqn 3) with IQR in error bars and (**b**) air temperature calculated with (eqn 9 - eqn 1) (no IQR as eqn 9 is linear). The EnergyPlus is used with the open terrain coefficients (Table 6). Analysis is for mid floor height with uTMY forcing.*

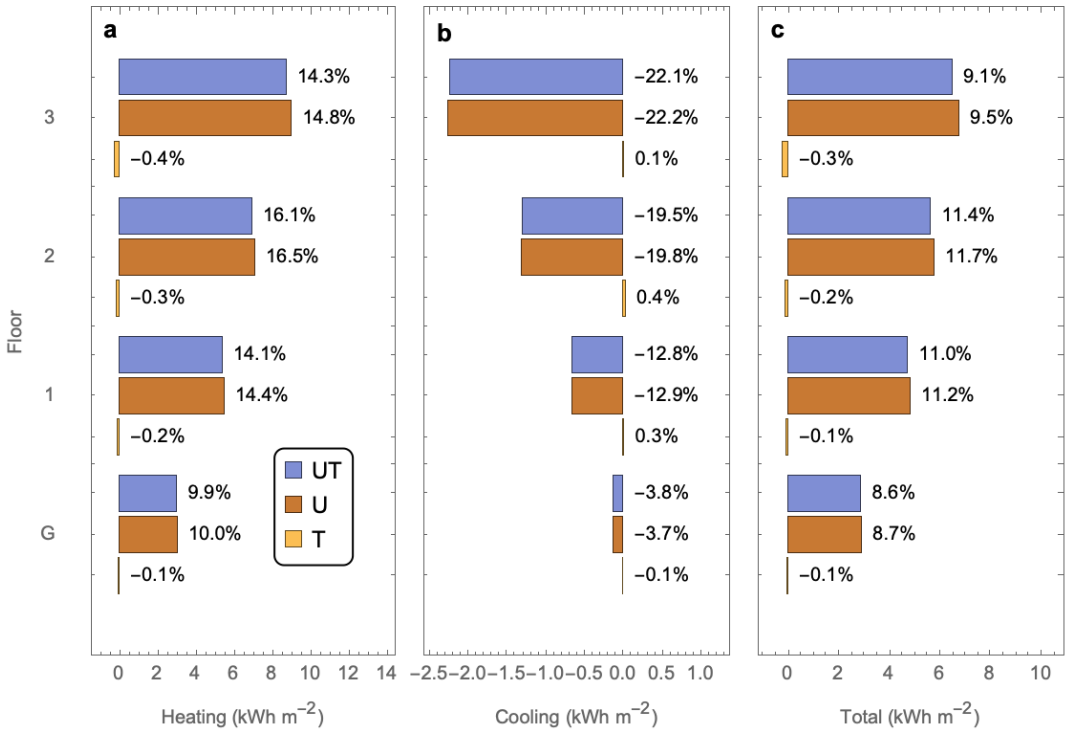

***Figure 11**: EnergyPlus simulated annual energy load using with new coefficients [UT, U, T] minus open terrain (default) (Table 6) for: (a) heating, (b) cooling and (c) total. Percentages (%) are differences normalised by the open terrain values.*

5 Concluding remarks

By using typical meteorological year (TMY) (or other similar weather data types) datasets with neighbourhood characteristics for use in building energy simulations the results should be more applicable to actual building settings. Our proposed method uses the SUEWS (Surface Urban Energy and Water Balance Scheme) urban land surface model with long-term (1979-2020) ERA5 climate data to generate an urban TMY (uTMY). Both uTMY and conventional TMY (cTMY) data are used to force EnergyPlus to determine the energy load for a four-storey building with flats in central London in heating-cooling mode.

It is concluded that:

- The wind speed values in the uTMY data are lower than the cTMY, whereas temperature and humidity differences are minimal as the data assimilation into the ERA5 dataset has acquired some of the urban thermal signature.
- Of these three meteorological variables, wind speed has the largest impact on building energy load.
- Using long-term ERA5 data with urban characteristics (uAMY) in London, the uTMY forced EnergyPlus energy load simulations fit better than cTMY. However, cTMY heating degree days (HDD) are closer to the uAMY median, while cooling degree days (CDD) of both cTMY and uTMY differ from the uAMY median. This suggests temperature-only indices may be inadequate proxies for determining energy load.
- Using the default (i.e., open terrain) parameters in EnergyPlus the vertical profiles forced with uTMY data modifies the annual both heating (11.5 % lower) and cooling (44.6% higher) energy loads (cf. cTMY).
- New wind speed (cf. air temperature) profile coefficients, derived with the SUEWS-RSL scheme, have a larger impact on predicted energy load. With greater impact at higher (cf. lower) floors. The difference in annual load can be ~10%.

This work highlights the importance of considering the neighbourhood climate for building energy simulation (Section 4.2), including the vertical heterogeneity as this influences intra-floor energy loads (Section 4.3). As we apply the uTMY approach to only one area, with minimal cooling needs, further studies should consider a wider range of climates, including future climate (i.e. replacing the ERA5 data with projections). The EnergyPlus terrain profile coefficients could be derived for a wider range of neighbourhoods types (e.g. with shorter/taller buildings, less/more dense) using the SUEWS-RSL.

There are clearly other improvements to EnergyPlus meteorological forcing that can be made. The most obvious is related to the radiation field to take into account the neighbourhood geometry. This is a focus of our recent work (e.g. Xie et al. 2021). It should be noted that changing the weights from those used in the TMY (Table A1), to those such as used in TRY (Eames et al., 2016), would likely make the impacts and benefits of our proposed method greater as the relative importance of solar radiation is decreased.

Acknowledgements

The support from EPSRC LoHCool (EP/N009797/1), NERC Independent Research Fellowship (NE/P018637/1), NERC COSMA (NE/S005889/1) and Newton Fund/ Met Office CSSP-China (SG, NT, ZL) are all gratefully acknowledged. Insightful comments from three anonymous reviewers are sincerely appreciated.

Appendix A: Generation of conventional Typical Meteorological Year (cTMY)

To generate a conventional TMY (cTMY) dataset, the 12 "best" months are selected from a "long-term" climatology to create a "typical year" (Fig. A1), in four steps (Herrera et al., 2017):

(*c1*) *Selection of key variables*: Meteorological observations (e.g., air temperature, air humidity, wind speed and solar radiation) relevant to building energy consumption (e.g., related to HVAC processes) are identified.

(*c2*) *Selection of a meteorological variables data source:* e.g., standard WMO weather station observations

(*c3*) *Assessment of representativeness* of each month (typically) uses closeness of a variable to the desired long-term climatology based on the Finkelstein and Schafer (1971) (F_v) metric:

$$F_v = \left(\frac{1}{n}\right)\sum_{i=1}^{n}|X_i - \bar{X}| \quad \text{(A1)}$$

where n is the number of daily readings in a month, i is the sequential position in variable record X_i in its cumulative distribution function (CDF) and $\bar{X}$ the mean rank of long-term CDF. The scores are combined with weights (w_v) (Table A1) for each variable's assessed impact on modelled HVAC (Hall et al., 1978):

$$W = \Sigma w_v F_v, \quad \text{(A2)}$$

As our aim is to modify the cTMY dataset with urban climate modelling rather than to correct the original methodology, we do not modify the weighing scheme (Table A1). However, others have adjusted them in some contexts (Su et al. 2009) and could explore these impacts within the uTMY framework in a future study.

(*c4*) *Selection of representative months* (Pissimanis et al. 1988) considers the five lowest *W* scores (of all the years) for each month. From the five candidates, given the importance of incoming solar radiation ($K_{\downarrow}$, Table A.1), the month selected for the *TMY* has the smallest root mean square difference ($RMSD_{K_{\downarrow}}^{m}$) from the long-term climatological mean ($\overline{D}_m$):

$$RMSD_{K_{\downarrow}}^{m} = \left[\left(\frac{1}{n}\right)\sum_{j=1}^{n}(D_j - \overline{D}_m)^2\right]^{0.5} \quad \text{(A3)}$$

where D_j the flux for each day j in a candidate month. Although the *RMSD* is biased by outliers potentially resulting in less accurate assessment of closeness of the variable of interest (Chai and Draxler 2014; Willmott et al. 2017), we retain it for consistency.

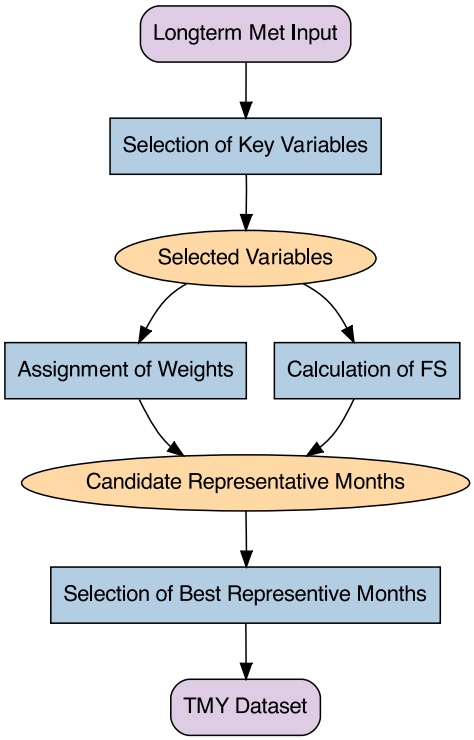

Figure A1*: Workflow to generate conventional typical meteorological year (cTMY) dataset.*

Table A1*: Weights (w) used (eqn A2) to generate a typical meteorological year (TMY) dataset (Hall et al., 1978).*

	Air temperature	Air relative humidity	Wind speed	Incoming solar radiation
mean	2/24	2/24	2/24	12/24
max	1/24	1/24	2/24	0
min	1/24	1/24	0	0

Appendix B: Height-based corrections of ERA5 forcing variables

For each ERA5 variable used to drive SUEWS corrections are undertaken. The heights referred to in the following equations are discussed in Section 3.1 (also shown in Fig. 1). The methods (with other original references) follow Weedon et al. (2010):

(1) ERA5 air temperature ($T_{2,E}$) at 2 m agl is used to obtain air temperature at the forcing height ($T_{s,U} = T_{2,E} + \Delta z_{net}\Gamma$) assuming an environmental lapse rate (Γ) of –6.5 K km^{-1}.

(2) Atmospheric pressure at the forcing height ($p_{S,U}$) is obtained using the hypsometric equation:

$$p_{s,U} = p_{2,E}\left(\frac{T_{2,E}}{T_{s,U}}\right)^{-\frac{g}{\Gamma R_d}} \quad \text{(B1)}$$

where g = 9.8 m s^{-2} is gravity acceleration, R_d = 287.05 J kg^{-1} K^{-2} is the ideal gas constant for dry air.

(3) Specific humidity $q_{S,U}$ is obtained assuming a constant relative humidity RH for Δz_S (Weedon et al. 2010, Kokkonen et al. 2018):

$$q_{s,U} = q_{sat,s,U}\,RH = q_{sat,s,U}\frac{q_{2,E}}{q_{sat,2,E}} \quad \text{(B2)}$$

where the saturation specific humidity (q_{sat}) at atmospheric pressure p is:

$$q_{sat} = \left(\frac{R_d}{R_v}\right)\frac{e_{sat}}{p - \left(1 - \frac{R_d}{R_v}\right)e_{sat}} \quad \text{(B3)}$$

where $R_v = 461.52$ J kg^{-1}K^{-1} the specific gas constant for dry air, and e_{sat} is the saturation vapour pressure at air temperature T is (Jones 2013):

$$e_{sat} = 613.75\exp\left(17.502 \times \frac{T - 273.15}{T - 32.18}\right) \quad \text{(B4)}$$

Eqn B3 and B4 are written generically for p and T at any height (i.e., without subscripts for height).

(4) Wind speed $U_{z,U}$ is determined using the log-law assuming neutral stability and ignoring u_* differences:

$$U_{s,U} = U_{10,E}\frac{\ln\left(\frac{\Delta z_{\text{net}} - z_{d,E}}{z_{0m,E}}\right)}{\ln\left(\frac{10_E - z_{d,E}}{z_{0m,E}}\right)}, \quad \text{(B5)}$$

References

Aliabadi, A. A., Krayenhoff, E. S., Nazarian, N., Chew, L. W., Armstrong, P. R., Afshari, A., and Norford, L. K.: Effects of roof-edge roughness on air temperature and pollutant concentration in urban canyons, Bound.-Lay. Meteorol., 164, 249–279, https://doi.org/10.1007/s10546-017-0246-1, 2017.

ASHRAE. International Weather for Energy Calculations (IWEC Weather Files) User's Manual and CD-ROM, Atlanta: ASHRAE, 2001.

ASHRAE: ASHRAE Handbook: Fundamentals - SI Edition. Atlanta, GA: American Society of Heating Refrigerating and Air-Conditioning, 2005.

Ao XY, CSB Grimmond, YY Chang, DW Liu, YQ Tang, P Hu, YD Wang, J Zou, JG Tan: Challenges of observing heat, water and carbon exchanges in Shanghai, a dense, tall megacity, Int. J. Climatology 36: 4608–4624, doi:10.1002/joc.4657, 2016.

Ao, X., Grimmond, C. S. B., Ward, H. C., Gabey, A. M., Tan, J., Yang, X.-Q., Liu, D., Zhi, X., Liu, H. and Zhang, N.: Evaluation of the Surface Urban Energy and Water balance Scheme (SUEWS) at a dense urban site in Shanghai: Sensitivity to anthropogenic heat and irrigation, J Hydrometeorol, JHM-D-18-0057.1, doi:10.1175/jhm-d-18-0057.1, 2018.

Beckman, W. A., Broman, L., Fiksel, A., Klein, S. A., Lindberg, E., Schuler, M. and Thornton, J.: TRNSYS the most complete solar energy system modeling and simulation software, Renewable Energy, 5(1-4), 486–488, doi:10.1016/0960-1481(94)90420-0, 1994.

Beijing Construction Bureau: Design standard for energy efficiency of public buildings., 2005.

Björkegren, A. and Grimmond, C.: Net carbon dioxide emissions from central London, Urban Clim, 23, 131–158, doi:10.1016/j.uclim.2016.10.002, 2018.

Bourikas, L.: Microclimate adapted localised weather data generation: Implications for urban modelling and the energy consumption of buildings, PhD thesis, University of Southampton., 2016.

Bragança, L., Vieira, S. M. and Andrade, J. B.: Early stage design decisions: The way to achieve sustainable buildings at lower costs, The Scientific World Journal, 2014, 1–8, doi:10.1155/2014/365364, 2014.

Broadbent, A. M., Coutts, A. M., Nice, K. A., Demuzere, M., Krayenhoff, E. S., Tapper, N. J. and Wouters, H.: The air-temperature response to green/blue-infrastructure evaluation tool (target v1.0): An efficient and user-friendly model of city cooling, Geoscientific Model Development, 12(2), 785–803, doi:10.5194/gmd-12-785-2019, 2019.

Brutsaert, W.: Evaporation into the atmosphere: Theory, history, and applications, Springer., 1982.

Campbell, G. S. and Norman, J. M.: An introduction to environmental biophysics, Springer New York, New York, NY., 1998.

Chai, T. and Draxler, R. R.: Root mean square error (RMSE) or mean absolute error (MAE)? – Arguments against avoiding RMSE in the literature, Geosci Model Dev, 7(3), 1247–1250, doi:10.5194/gmd-7-1247-2014, 2014.

Christen, A. and Vogt, R.: Energy and radiation balance of a central European city, Int J Climatol, 24(11), 1395–1421, doi:10.1002/joc.1074, 2004.

CIBSE: Environmental design: CIBSE guide A, CIBSE, London., 2006.

Cleugh, H. and Grimmond, S.: The Future of the World's Climate (Second Edition), Sect Anthropocene, 47–76, doi:10.1016/b978-0-12-386917-3.00003-8, 2012.

Communities and Local Government (2008) English House Condition Survey - 2006 Annual Report. London. Available at: https://www.gov.uk/government/collections/english-housing-survey.

Coumou, D. and Rahmstorf, S.: A decade of weather extremes, Nature Clim Change, 2(7), 491–496, doi:10.1038/nclimate1452, 2012.

Crank, P. J., Sailor, D. J., Ban-Weiss, G., and Taleghani, M.: Evaluating the ENVI-met microscale model for suitability in analysis of targeted urban heat mitigation strategies, Urban Clim., 26, 188–197, https://doi.org/10.1016/j.uclim.2018.09.002, 2018.

Crawley, D. B., Lawrie, L. K., Winkelmann, F. C., Buhl, W. F., Huang, Y., Pedersen, C. O., Strand, R. K., Liesen, R. J., Fisher, D. E., Witte, M. J. and Glazer, J.: EnergyPlus: Creating a new-generation building energy simulation program, Energy Build., 33(4), 319–331, doi:10.1016/s0378-7788(00)00114-6, 2001.

Cui, Y., Yan, D., Hong, T., Xiao, C., Luo, X. and Zhang, Q.: Comparison of typical year and multiyear building simulations using a 55-year actual weather data set from china, Appl. Energy, 195, 890–904, doi:10.1016/j.apenergy.2017.03.113, 2017.

Dastoor, A. P.: Cloudiness parameterization and verification in a large-scale atmospheric model, Tellus Dyn Meteorology Oceanogr, 46(5), 615–634, doi:10.3402/tellusa.v46i5.15648, 1994.

Dee, D. P., Balmaseda, M., Balsamo, G., Engelen, R., Simmons, A. J., and Thépaut, J.-N.: Toward a Consistent Reanalysis of the Climate System, B Am Meteorol Soc, 95, 1235–1248, https://doi.org/10.1175/bams-d-13-00043.1, 2014.

Duan, S., Luo, Z., Yang, X. and Li, Y.: The impact of building operations on urban heat/cool islands under urban densification: A comparison between naturally-ventilated and air-conditioned buildings, Appl Energ, 235, 129–138, doi:10.1016/j.apenergy.2018.10.108, 2019.

Dutra, E., Muñoz- Sabater, J., Boussetta, S., Komori, T., Hirahara, S. and Balsamo, G.: Environmental Lapse Rate for High- Resolution Land Surface Downscaling: An Application to ERA5, Earth Space Sci, 7(5), https://doi.org/10.1029/2019ea000984, 2020.

Eames, M., Ramallo-Gonzalez, A. and Wood, M.: An update of the UK's test reference year: The implications of a revised climate on building design, Build Serv Eng Res T, 37(3), 316–333, https://doi.org/10.1177/0143624415605626, 2016.

Finkelstein, J. M. and Schafer, R. E.: Improved goodness-of-fit tests, Biometrika, 58(3), 641, doi:10.2307/2334400, 1971.

Garratt, J. R.: Surface influence upon vertical profiles in the atmospheric near-surface layer, Quarterly Journal of the Royal Meteorological Society, 106(450), 803–819, doi:10.1002/qj.49710645011, 1980.

BEIS: Government leads energy charge across public sector, saving up to £340 million, [online] Available from: https://www.gov.uk/government/news/government-leads-energy-charge-across-public-sector-saving-up-to-340-million (Accessed 17 January 2020), 2018.

BEIS: Updated energy and emissions projections: 2018, [online] Available from: https://www.gov.uk/government/publications/updated-energy-and-emissions-projections-2018 (Accessed 17 January 2021), 2019.

Fatichi, S., Ivanov, V. Y. and Caporali, E.: Simulation of future climate scenarios with a weather generator, Adv Water Resour, 34(4), 448–467, doi:10.1016/j.advwatres.2010.12.013, 2011.

Forbes, R. M. and Ahlgrimm, M.: On the Representation of High-Latitude Boundary Layer Mixed-Phase Cloud in the ECMWF Global Model, Mon Weather Rev, 142(9), 3425–3445, doi:10.1175/mwr-d-13-00325.1, 2014.

Google: Google Earth Imagery, https://www.google.co.uk/maps (Accessed 3 May 2021), 2021.

Grimmond, C. S. B., Cleugh, H. A. and Oke, T. R.: An objective urban heat storage model and its comparison with other schemes, Atmospheric Environ Part B Urban Atmosphere, 25(3), 311 326, doi:10.1016/0957-1272(91)90003-w, 1991.

Grimmond, C. S. B. and Oke, T. R.: Urban water balance: 2. results from a suburb of vancouver, British Columbia, Water Resour. Res., 22(10), 1404–1412, doi:10.1029/wr022i010p01404, 1986.

Grimmond, C. S. B. and Oke, T. R.: An evapotranspiration-interception model for urban areas, Water Resour. Res., 27(7), 1739–1755, doi:10.1029/91wr00557, 1991.

Grimmond, C. S. B. and Oke, T. R.: Aerodynamic properties of urban areas derived from analysis of surface form, J. Appl. Meteor., 38(9), 1262–1292, doi:10.1175/1520-0450(1999)038<1262:apouad>2.0.co;2, 1999.

Grimmond, C. S. B. and Oke, T. R.: Turbulent heat fluxes in urban areas: Observations and a local-scale urban meteorological parameterization scheme (LUMPS), J. Appl. Meteor., 41(7), 792–810, doi:10.1175/1520-0450(2002)041<0792:thfiua>2.0.co;2, 2002.

Grimmond, C. S. B., Best, M., Barlow, J., Arnfield, A. J., Baik, J.-J., Baklanov, A., Belcher, S., Bruse, M., Calmet, I., Chen, F., Clark, P., Dandou, A., Erell, E., Fortuniak, K., Hamdi, R., Kanda, M., Kawai, T., Kondo, H., Krayenhoff, S., Lee, S. H., Limor, S.-B., Martilli, A., Masson, V., Miao, S., Mills, G., Moriwaki, R., Oleson, K., Porson, A., Sievers, U., Tombrou, M., Voogt, J., and Williamson, T.: Meteorological and Air Quality Models for Urban Areas, 97–123, https://doi.org/10.1007/978-3-642-00298-4_11, 2009.

Grimmond, C. S. B., Blackett, M., Best, M. J., Barlow, J., Baik, J. J., Belcher, S. E., Bohnenstengel, S. I., Calmet, I., Chen, F., Dandou, A., Fortuniak, K., Gouvea, M. L., Hamdi, R., Hendry, M., Kawai, T., Kawamoto, Y., Kondo, H., Krayenhoff, E. S., Lee, S.-H., Loridan, T., Martilli, A., Masson, V., Miao, S., Oleson, K., Pigeon, G., Porson, A., Ryu, Y.-H., Salamanca, F. P., Shashua-Bar, L., Steeneveld, G. J., Tombrou, M., Voogt, J. A., Young, D. T. and Zhang, N.: The International Urban Energy Balance Models Comparison Project: First Results from Phase 1, J Appl Meteorol Clim, 49(6), 1268 1292, doi:10.1175/2010jamc2354.1, 2010.

Grimmond, C. S. B., Blackett, M., Best, M. J., Baik, J. J., Belcher, S. E., Beringer, J., Bohnenstengel, S. I., Calmet, I., Chen, F., Coutts, A., Dandou, A., Fortuniak, K., Gouvea, M. L., Hamdi, R., Hendry, M., Kanda, M., Kawai, T., Kawamoto, Y., Kondo, H., Krayenhoff, E. S., Lee, S.-H., Loridan, T., Martilli, A., Masson, V., Miao, S., Oleson, K., Ooka, R., Pigeon, G., Porson, A., Ryu, Y.-H., Salamanca, F. P., Steeneveld, G. J., Tombrou, M., Voogt, J. A., Young, D. T. and Zhang, N.: Initial results from Phase 2 of the international urban energy balance model comparison, Int J Climatol, 31(2), 244 272, doi:10.1002/joc.2227, 2011.

Grohmann, C. H.: Evaluation of TanDEM-X DEMs on selected Brazilian sites: Comparison with SRTM, ASTER GDEM and ALOS AW3D30. Remote Sensing of Environment, 212, 121–133, doi:10.1016/j.rse.2018.04.043, 2018.

Gulvanessian, H., Calgaro, J.-A. and Holicky, M.: Designers' guide to eurocode: Basis of structural design., 2012.

Gupta, A. & Moss, P. Guidelines for design of low-rise buildings subjected to lateral forces. Boca Raton: CRC Press, 1993.

Harman, I. N. and Finnigan, J. J.: A simple unified theory for flow in the canopy and roughness sublayer, Bound-lay Meteorol, 123(2), 339–363, doi:10.1007/s10546-006-9145-6, 2007.

Harman, I. N. and Finnigan, J. J.: Scalar Concentration Profiles in the Canopy and Roughness Sublayer, Bound-lay Meteorol, 129(3), 323–351, doi:10.1007/s10546-008-9328-4, 2008.

Hall, I. J., Prairie, R. R., Anderson, H. E. and Boes, E. C.: Generation of Typical Meteorological Years for 26 SOLMET Stations, Sandia Laboratories., 1978.

Herrera, M., Natarajan, S., Coley, D. A., Kershaw, T., Ramallo-González, A. P., Eames, M., Fosas, D. and Wood, M.: A review of current and future weather data for building simulation, Build. Serv. Eng. Res. Technol., 38(5), 602–627, doi:10.1177/0143624417705937, 2017.

Hersbach, H., Bell, B., Berrisford, P., Hirahara, S., Horányi, A., Muñoz- Sabater, J., Nicolas, J., Peubey, C., Radu, R., Schepers, D., Simmons, A., Soci, C., Abdalla, S., Abellan, X., Balsamo, G., Bechtold, P., Biavati, G., Bidlot, J., Bonavita, M., Chiara, G., Dahlgren, P., Dee, D., Diamantakis, M., Dragani, R., Flemming, J., Forbes, R., Fuentes, M., Geer, A., Haimberger, L., Healy, S., Hogan, R. J., Hólm, E., Janisková, M., Keeley, S., Laloyaux, P., Lopez, P., Lupu, C., Radnoti, G., Rosnay, P., Rozum, I., Vamborg, F., Villaume, S. and Thépaut, J.: The ERA5 global reanalysis, Q J Roy Meteor Soc, doi:10.1002/qj.3803, 2020.

Hong, T., Chang, W.-K. and Lin, H.-W.: A fresh look at weather impact on peak electricity demand and energy use of buildings using 30-year actual weather data, Appl Energ, 111, 333–350, doi:10.1016/j.apenergy.2013.05.019, 2013.

Hong, T., Chen, Y., Luo, X., Luo, N. and Lee, S. H.: Ten questions on urban building energy modeling, Build Environ, 168, 106508, doi:10.1016/j.buildenv.2019.106508, 2020.

IEA: Global energy & CO2 status report, [online] Available from: https://www.iea.org/geco/ (Accessed 17 January 2020), 2019.

Järvi, L., Grimmond, C. S. B. and Christen, A.: The surface urban energy and water balance scheme (SUEWS): Evaluation in Los Angeles and Vancouver, J. Hydrol., 411(3-4), 219–237, doi:10.1016/j.jhydrol.2011.10.001, 2011.

Järvi, L., Grimmond, C. S. B., Taka, M., Nordbo, A., Setälä, H. and Strachan, I. B.: Development of the surface urban energy and water balance scheme (SUEWS) for cold climate cities, Geosci. Model Dev., 7(4), 1691–1711, doi:10.5194/gmd-7-1691-2014, 2014.

Jones, H.: Plants and Microclimate: A Quantitative Approach to Environmental Plant Physiology. Cambridge: Cambridge University Press. doi:10.1017/CBO9780511845727, 2013.

Kawai, T., Ridwan, M. K. and Kanda, M.: Evaluation of the simple urban energy balance model using selected data from 1-yr flux observations at two cities, J. Appl. Meteor. Climatol., 48(4), 693–715, doi:10.1175/2008jamc1891.1, 2009.

Kent, C. W., Grimmond, C. S. B., Gatey, D. and Hirano, K.: Urban morphology parameters from global digital elevation models: Implications for aerodynamic roughness and for wind-speed estimation, Remote Sens Environ, 221, 316–339, doi:10.1016/j.rse.2018.09.024, 2019.

Kershaw, T., Sanderson, M., Coley, D. and Eames, M.: Estimation of the urban heat island for UK climate change projections, Build Serv Eng Res T, 31(3), 251–263, doi:10.1177/0143624410365033, 2010.

Kokkonen, T. V., Grimmond, C. S. B., Räty, O., Ward, H. C., Christen, A., Oke, T. R., Kotthaus, S. and Järvi, L.: Sensitivity of Surface Urban Energy and Water Balance Scheme (SUEWS) to downscaling of reanalysis forcing data, Urban Clim, 23(Urban Clim. 13 2015), 36 52, doi:10.1016/j.uclim.2017.05.001, 2018.

Kokkonen, T. V., Grimmond, C. S. B., Murto, S., Liu, H., Sundström, A.-M. and Järvi, L.: Simulation of the radiative effect of haze on the urban hydrological cycle using reanalysis data in Beijing, Atmos Chem Phys, 19(10), 7001 7017, doi:10.5194/acp-19-7001-2019, 2019.

Kondo, H., Genchi, Y., Kikegawa, Y., Ohashi, Y., Yoshikado, H. and Komiyama, H.: Development of a Multi-Layer Urban Canopy Model for the Analysis of Energy Consumption in a Big City: Structure of the Urban Canopy Model and its Basic Performance, Bound-lay Meteorol, 116(3), 395–421, doi:10.1007/s10546-005-0905-5, 2005.

Kotthaus, S. and Grimmond, C. S. B.: Energy exchange in a dense urban environment – Part II: Impact of spatial heterogeneity of the surface, Urban Clim, 10, 281 307, doi:10.1016/j.uclim.2013.10.001, 2014.

Kotthaus, S. and Grimmond, C. S. B.: Atmospheric boundary- layer characteristics from ceilometer measurements. Part 2: Application to London's urban boundary layer, Q J Roy Meteor Soc, 144(714), 1511–1524, doi:10.1002/qj.3298, 2018.

Lindberg, F., Onomura, S. and Grimmond, C. S. B.: Influence of ground surface characteristics on the mean radiant temperature in urban areas, Int J Biometeorol, 60(9), 1 14, doi:10.1007/s00484-016-1135-x, 2016.

Liu, H., Gong, P., Wang, J., Wang, X., Ning, G., and Xu, B.: Production of global daily seamless data cubes and quantification of global land cover change from 1985 to 2020 - iMap World 1.0, Remote Sens Environ, 258, 112364, https://doi.org/10.1016/j.rse.2021.112364, 2021.

Loridan, T., Grimmond, C. S. B., Offerle, B. D., Young, D. T., Smith, T. E. L., Järvi, L. and Lindberg, F.: Local-Scale Urban Meteorological Parameterization Scheme (LUMPS): Longwave Radiation Parameterization and Seasonality-Related Developments, J Appl Meteorol Clim, 50(1), 185 202, doi:10.1175/2010jamc2474.1, 2011.

Lokmanhekim, M., Winkelmann, F., Rosenfeld, A., Cumali, Z., Leighton, G. and Ross, H.: DOE-2: A new state-of-the-art computer program for the energy utilization analysis of buildings, Lawrence Berkeley Lab. Report CBC-8977, Berkeley, California, 1979.

Loridan, T.: Evaluation and developments to urban land surface modelling: Offline and online, PhD thesis, King's College London., 2011.

Lowry, W. P.: Empirical Estimation of Urban Effects on Climate: A Problem Analysis, J Appl Meteorol, 16(2), 129–135, doi:10.1175/1520-0450(1977)016<0129:eeoueo>2.0.co;2, 1977.

Mauder, M., Foken, T. and Cuxart, J.: Surface-Energy-Balance Closure over Land: A Review, Bound-lay Meteorol, 1–32, doi:10.1007/s10546-020-00529-6, 2020.

Meggers, F., Leibundgut, H., Kennedy, S., Qin, M., Schlaich, M., Sobek, W. and Shukuya, M.: Reduce CO2 from buildings with technology to zero emissions, Sustainable Cities and Society, 2(1), 29–36, doi:10.1016/j.scs.2011.10.001, 2012.

Meili, N., Manoli, G., Burlando, P., Bou-Zeid, E., Chow, W. T. L., Coutts, A. M., Daly, E., Nice, K. A., Roth, M., Tapper, N. J., Velasco, E., Vivoni, E. R. and Fatichi, S.: An urban ecohydrological model to quantify the effect of vegetation on urban climate and hydrology (UT&C v1.0), Geoscientific Model Development, 13(1), 335–362, doi:10.5194/gmd-13-335-2020, 2020.

Miguel, A. de and Bilbao, J.: Test reference year generation from meteorological and simulated solar radiation data, Sol. Energy, 78(6), 695–703, doi:10.1016/j.solener.2004.09.015, 2005.

MOHURD: Thermal design code of civil buildings (GB 50176-93), The Ministry of Housing; Urban-Rural Development of People's Republic of China., 2016.

Monin, A. and Obukhov, A. M.: Basic laws of turbulent mixing in the surface layer of the atmosphere, Trudy Geofiz. Inst. Acad. Nauk SSSR, 24(151), 163–187, 1954.

Murphy, J.: Predictions of climate change over Europe using statistical and dynamical downscaling techniques, Int J Climatol, 20(5), 489–501, doi:10.1002/(sici)1097-0088(200004)20:5<489::aid-joc484>3.0.co;2-6, 2000

Nazi, W. I. W. M., Royapoor, M., Wang, Y. and Roskilly, A. P.: Office building cooling load reduction using thermal analysis method – A case study, Appl Energ, 185, 1574–1584, doi:10.1016/j.apenergy.2015.12.053, 2017.

Nik, V. M.: Making energy simulation easier for future climate – synthesizing typical and extreme weather data sets out of regional climate models (RCMs), Appl. Energy, 177, 204–226, doi:10.1016/j.apenergy.2016.05.107, 2016.

Offerle, B., Grimmond, C. S. B. and Oke, T. R.: Parameterization of net all-wave radiation for urban areas, J. Appl. Meteor., 42(8), 1157–1173, doi:10.1175/1520-0450(2003)042<1157:ponarf>2.0.co;2, 2003.

Offerle, B., Jonsson, P., Eliasson, I. and Grimmond, C. S. B.: Urban Modification of the Surface Energy Balance in the West African Sahel: Ouagadougou, Burkina Faso, J Climate, 18(19), 3983–3995, doi:10.1175/jcli3520.1, 2005.

Ohunakin, O. S., Adaramola, M. S., Oyewola, O. M. and Fagbenle, R. O.: Generation of a typical meteorological year for north–east, Nigeria, Appl. Energy, 112, 152–159, doi:10.1016/j.apenergy.2013.05.072, 2013.

Oke, T. R., Mills, G., Christen, A. and Voogt, J. A.: Urban climates, Cambridge University Press, 2017.

OpenStreetMap contributors: OpenStreetMap, https://www.openstreetmap.org/(Accessed 3 May 2021), 2017.

Porritt, S.M., 2012. Adapting UK Dwellings for Heat Waves. PhD thesis, De Montfort University, Leicester

Ren, C., Cai, M., Li, X., Shi, Y. and See, L.: Developing a rapid method for 3-dimensional urban morphology extraction using open-source data, Sustainable Cities and Society, 101962, doi:10.1016/j.scs.2019.101962, 2019.

Ren, G., Zhou, Y., Chu, Z., Zhou, J., Zhang, A., Guo, J. and Liu, X.: Urbanization Effects on Observed Surface Air Temperature Trends in North China, J Climate, 21(6), 1333–1348, doi:10.1175/2007jcli1348.1, 2008.

Resler, J., Krˇc, P., Belda, M., Juruš, P., Benešová, N., Lopata,J., Vlˇcek, O., Damašková, D., Eben, K., Derbek, P., Maronga,B., and Kanani-Sühring, F.: PALM-USM v1.0: A new ur-ban surface model integrated into the PALM large-eddysimulation model, Geosci. Model Dev., 10, 3635–3659,https://doi.org/10.5194/gmd-10-3635-2017, 2017.

Salamanca, F. P., Krpo, A., Martilli, A. and Clappier, A.: A new building energy model coupled with an urban canopy parameterization for urban climate simulations—part I. formulation, verification, and sensitivity analysis of the model, Theor Appl Climatol, 99(3–4), 331 344, doi:10.1007/s00704-009-0142-9, 2009.

Sánchez, M. N., Soutullo, S., Olmedo, R., Bravo, D., Castaño, S. and Jiménez, M. J.: An experimental methodology to assess the climate impact on the energy performance of buildings: A ten-year evaluation in temperate and cold desert areas, Appl Energ, 264, 114730, doi:10.1016/j.apenergy.2020.114730, 2020.

Schleussner, C.-F., Rogelj, J., Schaeffer, M., Lissner, T., Licker, R., Fischer, E. M., Knutti, R., Levermann, A., Frieler, K. and Hare, W.: Science and policy characteristics of the Paris agreement temperature goal, Nature Clim Change, 6(9), 827–835, doi:10.1038/nclimate3096, 2016.

Strachan, P. A., Kokogiannakis, G. and Macdonald, I. A.: History and development of validation with the ESP-r simulation program, Build. Environ., 43(4), 601–609, doi:10.1016/j.buildenv.2006.06.025, 2008.

Su, F., Huang, J., Xu, T. and Zhang, C.: An evaluation of the effects of various parameter weights on typical meteorological years used for building energy simulation, Build Simul-china, 2(1), 19–28, doi:10.1007/s12273-009-9106-3, 2009.

Sun, T. and Grimmond, S.: A python-enhanced urban land surface model SuPy (SUEWS in python, v2019.2): Development, deployment and demonstration, Geosci. Model Dev. Discuss., 2019, 1–24, doi:10.5194/gmd-2019-39, 2019.

Sun, T., Järvi, L., Omidvar, H., Theeuwes, N., Lindberg, F., Li, Z., and Grimmond, S.: Urban-Meteorology-Reading/SUEWS: 2020a Release (Version 2020a). Zenodo. http://doi.org/10.5281/zenodo.3828525 (Accessed 14 May 2020), 2020.

Sun, T., Tang, Y., Xie, X., Luo, Z., and Grimmond, S.: Data files of Tang et al. (2021, BAE). Zenodo. http://doi.org/10.5281/zenodo.4872459 (Accessed 30 May 2021), 2021.

Short, C. A., Lomas, K. J. and Woods, A.: Design strategy for low-energy ventilation and cooling within an urban heat island, Build Res Information, 32(3), 187 206, doi:10.1080/09613210410001679875, 2004.

Tan, J., Zheng, Y., Tang, X., Guo, C., Li, L., Song, G., Zhen, X., Yuan, D., Kalkstein, A. J., Li, F. and Chen, H.: The urban heat island and its impact on heat waves and human health in shanghai, Int J Biometeorol, 54(1), 75–84, doi:10.1007/s00484-009-0256-x, 2009.

Theeuwes, N. E., Ronda, R. J., Harman, I. N., Christen, A. and Grimmond, C. S. B.: Parametrizing Horizontally-Averaged Wind and Temperature Profiles in the Urban Roughness Sublayer, Boundary-Layer Meteorology, 173(3), 1–28, doi:10.1007/s10546-019-00472-1, 2019.

Theeuwes, N. E., Barlow, J. F., Teuling, A. J., Grimmond, C. S. B. and Kotthaus, S.: Persistent cloud cover over mega-cities linked to surface heat release, Npj Clim Atmospheric Sci, 2(1), 15, doi:10.1038/s41612-019-0072-x, 2019.

Three Regions Climate Change Group: Your home in a changing climate. London. http://climatelondon.org/. (Accessed 22 Feb 2021), 2008.

Varquez, A. C. G., Kiyomoto, S., Khanh, D. N., and Kanda, M.: Global 1-km present and future hourly anthropogenic heat flux, Sci Data, 8, 64, https://doi.org/10.1038/s41597-021-00850-w, 2021.

Wang, L., Liu, J., Gao, Z., Li, Y., Huang, M., Fan, S., Zhang, X., Yang, Y., Miao, S., Zou, H., Sun, Y., Chen, Y., Yang, T.: Vertical observations of the atmospheric boundary layer structure over Beijing urban area during air pollution episodes Atmospheric Chemistry and Physics 19(10), 6949-6967, doi:10.5194/acp-19-6949-2019, 2019

Ward, H. C. and Grimmond, C. S. B.: Assessing the impact of changes in surface cover, human behaviour and climate on energy partitioning across Greater London, Landscape Urban Plan, 165, 142 161, doi:10.1016/j.landurbplan.2017.04.001, 2017.

Ward, H. C., Kotthaus, S., Järvi, L. and Grimmond, C. S. B.: Surface urban energy and water balance scheme (SUEWS): Development and evaluation at two UK sites, Urban Clim., 18, 1–32, doi:10.1016/j.uclim.2016.05.001, 2016.

Warren, E., Charlton-Perez, C., Kotthaus, S., Marenco, F., Ryder, C., Johnson, B., Green, D., Lean, H., Ballard, S., Grimmond, S.: Observed aerosol characteristics to improve forward-modelled attenuated backscatter in urban areas Atmospheric Environment 224, 117177., doi:10.1016/j.atmosenv.2019.117177, 2020

Warren, E., Charlton-Perez, C., Kotthaus, S., Lean, H., Ballard, S., Hopkin, E., Grimmond, S.: Evaluation of forward-modelled attenuated backscatter using an urban ceilometer network in London under clear-sky conditions Atmospheric Environment 191, 532-547, doi:10.1016/j.atmosenv.2018.04.045, 2018

Weedon, G. P., Gomes, S., Viterbo, P., Shuttleworth, W. J., Blyth, E., Österle, H., Adam, J. C., Bellouin, N., Boucher, O. and Best, M.: Creation of the WATCH Forcing Data and Its Use to Assess Global and Regional Reference Crop Evaporation over Land during the Twentieth Century, J Hydrometeorol, 12(5), 823–848, doi:10.1175/2011jhm1369.1, 2011.

Willmott, C. J., Robeson, S. M., and Matsuura, K.: Climate and other models may be more accurate than reported, Eos, 98, doi:10.1029/2017EO074939

WMO: Guide to meteorological instruments and methods of observation, World Meteorological Organisation., 2017.

Wolfram Research: NonlinearModelFit, Wolfram Language function, https://reference.wolfram.com/language/ref/NonlinearModelFit.html. (Accessed 17 January 2021), 2008.

Xie, X., Luo, Z., Grimmond, S., Sun, T., Impact of inter-building longwave radiative exchanges on building energy performance and indoor overheating, Energy and Buildings, under review.

Xiong, J., Yao, R., Grimmond, S., Zhang, Q. and Li, B.: A hierarchical climatic zoning method for energy efficient building design applied in the region with diverse climate characteristics, Energy Build., 186, 355–367, doi:10.1016/j.enbuild.2019.01.005, 2019.

Yang, L., Yan, H. and Lam, J. C.: Thermal comfort and building energy consumption implications – a review, Appl. Energy, 115, 164–173, doi:10.1016/j.apenergy.2013.10.062, 2014.

Yao, R., Luo, Q. and Li, B.: A simplified mathematical model for urban microclimate simulation, Build Environ, 46(1), 253–265, doi:10.1016/j.buildenv.2010.07.019, 2011.

Yao, R., Luo, Q., Luo, Z., Jiang, L. and Yang, Y.: An integrated study of urban microclimates in Chongqing, China: Historical weather data, transverse measurement and numerical simulation, Sustain Cities Soc, 14, 187–199, doi:10.1016/j.scs.2014.09.007, 2015.

Yao, R., Costanzo, V., Li, X., Zhang, Q. and Li, B.: The effect of passive measures on thermal comfort and energy conservation. A case study of the hot summer and cold winter climate in the Yangtze River region, J Build Eng, 15, 298–310, doi:10.1016/j.jobe.2017.11.012, 2018.

Zang, H., Wang, M., Huang, J., Wei, Z. and Sun, G.: A hybrid method for generation of typical meteorological years for different climates of china, Energies, 9(12), 1094, doi:10.3390/en9121094, 2016.

Zhang Q. and Huang J.: Chinese Typical Year Weather Data for Architectural Use. China Machine Press. 2004 (in Chinese)

Supplementary Material

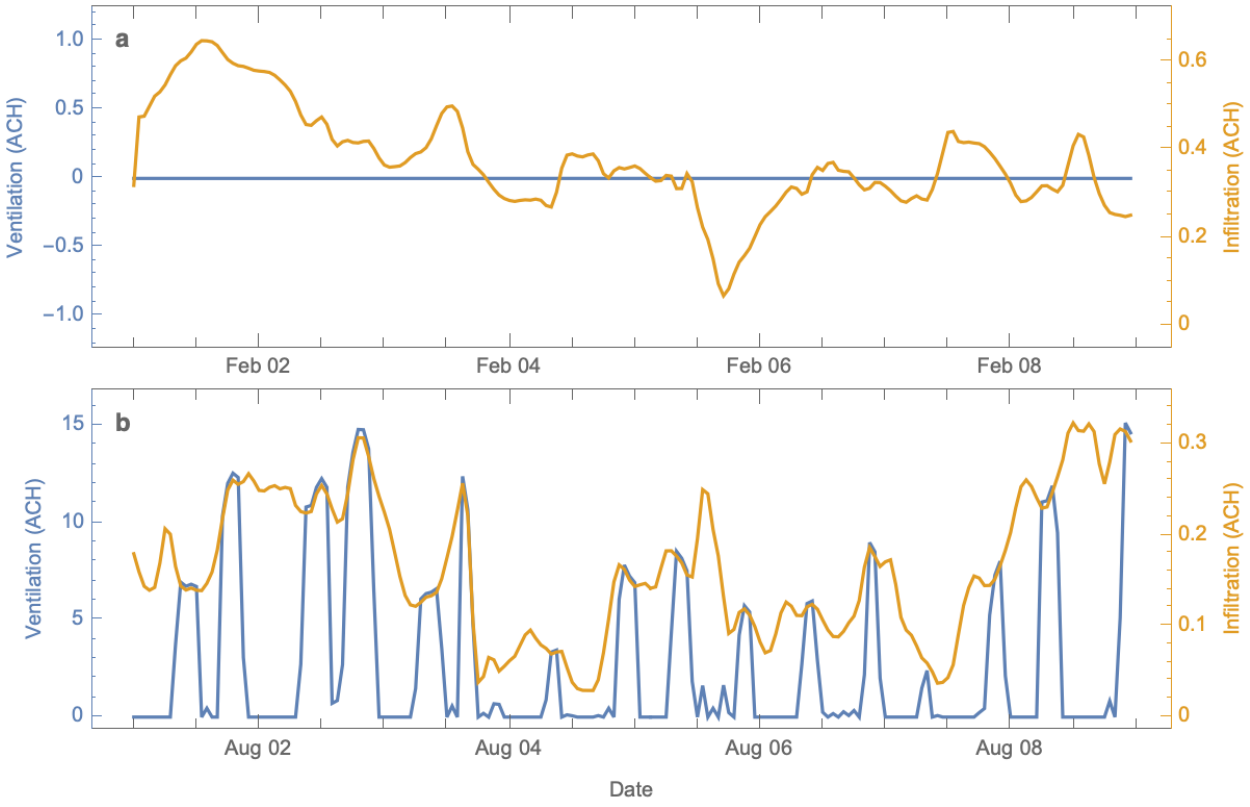

***Figure S1**: EnergyPlus simulated ventilation (blue, left y axis) and infiltration (orange, right y axis) driven by the uTMY dataset for two typical periods: a) winter (01 Feb – 08 Feb) and b) summer (01 Aug – 08 Aug).*

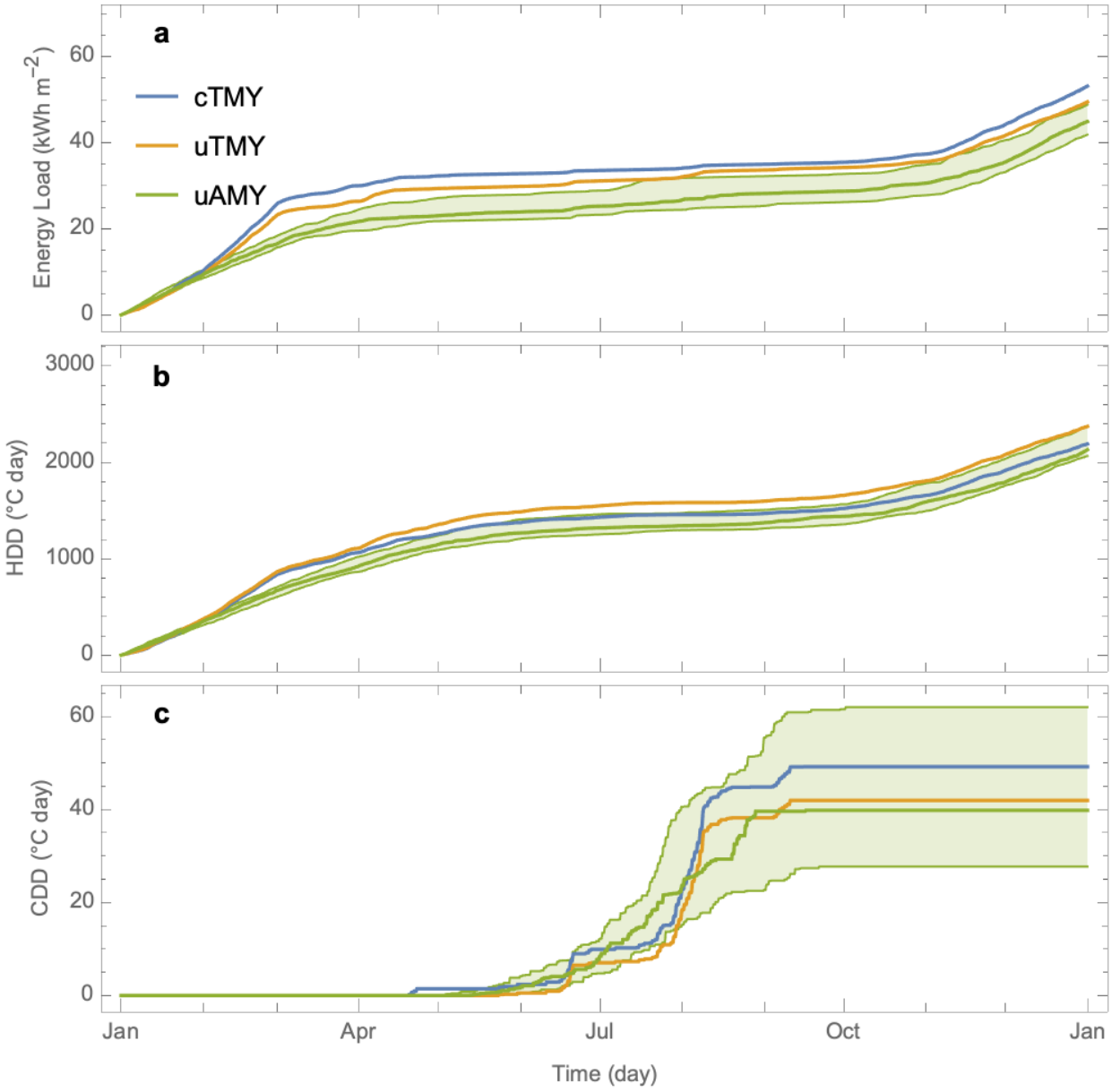

***Figure S2**: Using cTMY, uTMY and uAMY (multi-year median (line) and inter-quartile range (shading)) to determine cumulative: (a) total energy load, (b) heating degree days (HDD) and (c) cooling degree days (CDD).*